*Master Thesis*

# Electric motor installation for improved vehicle noise characteristics

*Jesper Schwartz*

*Division of Machine Design • Department of Design Sciences*

*Faculty of Engineering LTH • Lund University • 2014*


LUND UNIVERSITY

# Electric motor installation for improved vehicle noise characteristics

*Jesper Schwartz*

*Division of Machine Design • Department of Design Sciences*

*Faculty of Engineering LTH • Lund University • 2014*

Division of Machine Design, Department of Design Sciences
Faculty of Engineering LTH, Lund University
P.O. Box 118
SE-221 00 Lund
Sweden

ISRN LUTMDN/TMKT 14/5500 SE

# Preface

This master thesis is the last part of my education at the Division of machine design at Lund University. It was carried out at the NVH Center at Volvo Cars in Gothenburg where most of the work was done.

Firstly, I would like to thank my supervisors at Volvo, Magnus Olsson and Per Alenius, for always answering the endless questions that came up during the thesis and helping me discuss the topics and ideas. A special thanks to David Lennström for helping me with the measurements. Furthermore I would like to thank the rest of the staff at the NVH Center for encouraging my work and giving me a great experience during the project.

I would like to thank my academic supervisor Per Kristav for the guidance through the project.

Finally, thanks to my family and friends who always have supported me.

Lund, June 2014

Jesper Schwartz

# Abstract

As hybrid vehicles are growing more popular, new challenges for manufacturers arise to achieve good NVH. This master thesis analyzes an electric motor installation at the rear axle on the Volvo V60 Plug-in Hybrid with the goal to lower the noise level in the vehicle compartment. Measurements are combined with CAE-analyses to understand the problem areas and the behavior of the existing installation. Five concept layouts were generated and evaluated were one showed a lower noise level. This layout was further designed with regard to space limitations on a concept level which could be implemented as a proof-of-concept in an existing vehicle.

**Keywords:**

NVH, CAE, hybrid, acoustics

# Sammanfattning

Det här projektet utfördes i samarbete med Volvo Cars i Göteborg som ville utreda en elmotorinstallation med avseende på att förbättra dess ljudegenskaper. Projektet baseras på elmotorinstallationen i nuvarande V60 Hybrid vilken har en elmotor med integrerad planetväxel och differential monterad på bakre subframe. Bilar med elmotorer är en relativt ny utmaning för biltillverkare då beteendet skiljer sig mot bilar med konventionella förbränningsmotorer som har dominerat marknaden under de senaste årtiondena. Elmotorerna är ofta lättare än förbränningsmotorer vilket flyttar upp det problematiska frekvensområdet. Problemet som analyseras är att ett lågfrekvent vinande s.k. ”spårvagnsljud” vars frekvens ökar med hastighet och uppstår vid acceleration i elektriskt körläge. Detta uppstår på grund av ett momentrippel vilket beror på kombinationen av slottar och poler i elmotorn. Tillvägagångssättet bestod av mätningar, konceptgenerering, CAE-analyser samt en konstruktionsprocess. Mätningar utfördes i två steg. De opererande mätningarna gjordes vid långsam acceleration uppför en backe och samtidigt spelades interiörljud och accelerationer på bakre subframe in. Dessa kompletterades med stillastående mätningar med bilen på billyft där överföringsfunktioner mättes mellan infästningspunkter, subframe samt interiör. Det visade sig att tre strukturburna motorordningar uppstod, 10, 30 och 90 i frekvensområdet 50 till 300 Hz. En inledningsvägsanalys visade att z-riktningen för elmotorns fästpunkter var den dominerande källan. Fem olika koncept genererades med begränsningen att grundstrukturen på existerande subframe behölls. Mätdatan användes för att beräkna krafterna som uppstod vid infästningspunkterna för den nuvarande installationen. Dessa applicerades i CAE-modellen för att jämföras med en enhetslast som applicerades på elmotorns tyngdpunkt runt y-axeln. Detta för att hitta en enhetslast som överensstämmer med momentripplet och för att senare kunna jämföra koncepten mot varandra. Koncepten modellerades i beräkningsmodellen och utvärderades genom att jämföra ljudnivån i kupén. Ett av koncepten påvisade betydligt lägre ljudnivå än de övriga och valdes för vidareutveckling. Konceptet konstruerades i ett CAD-program och ritades så att den nuvarande elmotorns infästningspunkter på statorhuset kan användas. Det som tillkommer utöver ramen är fästen på sidor och en nedre rörelsebegränsare. Positionerna för infästningarna på sidorna justerades uppåt mot den grundläggande idén för att skapa frigång för drivaxlarnas inre medbringare vilka visade sig vara i vägen. Detta visade sig ha negativ påverkan på ljudnivån interiört vilken ökade något. För att få reda hur konceptet beter sig under extrema lastförhållanden jämfört med den nuvarande installationen användes en ADAMS-modell. Bilen utsattes för ett lastfall där den gavs en initial hastighet på halt väglag

och efter en bestämd tid låstes bromsarna. Konceptet påvisade stora rörelser i bussningarna (>7.5mm) vilket föranledde en studie i hur mycket uppvridning och förskjutning som kan tillåtas. Detta beror till stor del på de krav som satts upp av körbarhet och hur mycket utrymme som finns tillgängligt i bilen. Elmotorn frilades och ett Matlab-skript skrevs för att kunna jämföra statisk uppvridning och bussningsförskjutning med pålagt moment. Uppvridningen för konceptet blev 4.9˚ jämfört med den nuvarande installationen vars maximala uppvridning 1.3˚. Resultaten visade att ljudnivån är starkt relaterad mot tillåten uppvridning. Lägre tillåten uppvridning ger ökande ljudnivå i kupén. En jämförelse mellan den nuvarande installationen och konceptet där 1.3˚ tillåts för båda visar att konceptet ger upphov till en högre ljudnivå upp till 63 Hz. Mellan 63 till 150 Hz uppnås en lägre ljudnivå med konceptet. Tillåts båda installationerna att vridas upp 4.9˚ så visade konceptet en något högre ljudnivå upp till 50 Hz. Från 50 Hz och uppåt blir ljudnivån lägre. Slutsatsen är att ljudnivån i bil är beroende dels på tillåten uppvridning men även på installationens utformning.

# Table of Contents

# 1 Introduction

*This chapter introduces the reader to the background, scope and a method description of the project. Furthermore it contains a description of the limitations.*

## 1.1 Background

A growing interest among vehicle manufacturers towards developing vehicles that emit fewer emissions has led to more installations of hybrid- and electric powertrains. Legislations have made vehicles that emit low emissions popular on the market causing a customer interest in more environmental friendly cars. Customer demands increase simultaneously and the vehicles overall quality and sounds are becoming more important to be proven as a premium car manufacturer.

The sound and vibration characteristics of electric motors differ compared to internal combustion powertrains. These emit for example booming and combustion noise while electric motors emit more buzzing and whining noise, causing new challenges for manufacturers. This thesis arose due to a phenomenon called “tram noise” which is a low-frequency whining noise that occurs at low speed driving conditions in electric mode. The problem is installation dependent and therefore the electric motor installation layout is studied.

## 1.2 Scope

In this work an installation of electric motor at the rear axle will be studied. The work will investigate an installation for rubber bushing position and characteristics to get the lowest possible noise transfer into the vehicle compartment. Measurements of the rear axle electric motor will be used in combination with simulation models of the vehicle to better understand different types of installation concepts. The assembled rear axle including the electric motor is seen in figure 1.2-1.

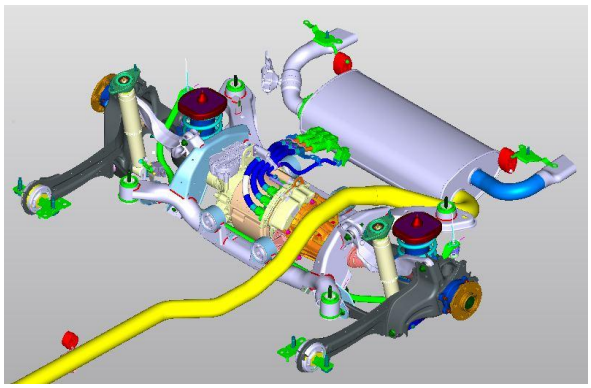

**Figure 1.2-1** Assembled rear axle with electric motor mounted in the subframe

## 1.3 Aims

The aim of this thesis is to find an installation for an electric motor that transfers less noise into the vehicle compartment than the existing layout.

The following topics are investigated to achieve this:

- Which noise levels exist?
- Study of the existing installation
- Concept generation
- CAE study and concept selection
- Concept design

## 1.4 Method description

Firstly, measurements were performed to understand the noise problem and generate input data for the CAE analysis. Thereafter the existing installation was analyzed and possible concept layouts were generated. The concepts were built in the CAE model and the comparison was done by applying a unit load that approximately corresponds to the measured forces. One concept showed lower sound pressure levels than the others and was therefore chosen for further development. The first development part was designing an installation that actually is possible to realize. Furthermore the concept design was analyzed using an ADAMS model and finally a windup study was made. An overview of the work flow is shown in figure 1.4-1.

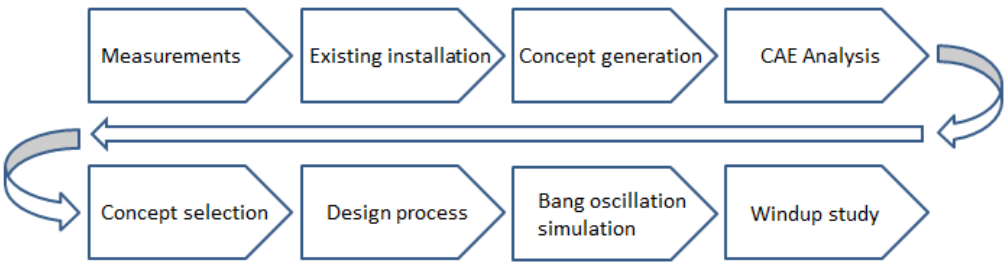


**Figure 1.4-1** Method description

## 1.5 Limitations

The installation analyzed in this thesis is limited to the existing model fleet and its corresponding properties. The noise transferred into the vehicle compartment depends on vehicle design and therefore the noise problem may differ for other electric motors and their installations in other vehicles. Furthermore it is assumed throughout that dimensioning regarding strength, fatigue and mount design is possible and can be done in future work. Concept designs are limited to the available design space, due to eventual implementation in future work (see chapter 3.5).

## 1.6 Nomenclature

AWD - All wheel drive

CAN – Controller area network

CoG – Center of gravity

ERAD – Electric rear axle drive

ICE – Internal combustion engine

IntM1 – Interior microphone 1 (driver's ear)

LMS – Leuven Measurement Systems International

NTF – Noise transfer function

NVH – Noise, vibration and harshness

PMSM – Permanent magnet synchronous machine

RPM – Revolutions per minute

RSS – Root sum square

SNR – Signal to noise ratio

SPL – Sound pressure level

TRA – Torque roll axis

# 2 Literature study

*This chapter contains a short theoretical background.*

## 2.1 NVH

NVH is an abbreviation for Noise, Vibration and Harshness and is one of the key attributes for vehicles today. NVH is considered as critical to obtain good comfort and usability for the end customer [1] and [2]. NVH consists of several areas i.e. powertrain-, road-, wind- and operational, which together are tuned to obtain the correct sound character for the specific vehicle according to set targets and legal requirements. The powertrain is the major contributor to noise and vibrations in the vehicle compartment but also wind- and road noise is a large contributor to the overall sound levels. Squeak and rattle is also important to control to obtain an overall good NVH experience.

## 2.2 Sound generation in electric motors

Electric motors convert electric energy to kinetic energy and as a side effect of this process, noise and vibrations are produced. The magnetic flux that crosses the air gap between the stator and rotor causes radial and tangential forces. Radial forces are the main source and cause the stator housing to vibrate and emit noise. Vibrations from the stator housing are either transferred through its mountings and affect the receiving structure or airborne causing surrounding air to fluctuate. Mechanical noise is caused by torque ripple that excites gears and couplings downstream from the motor. The torque ripple is coupled to motor orders that depend on the combination of slots and poles in the motor [3].

## 2.3 Acoustics of hybrid vehicles

To fulfill the requirements of emitted noise and customer satisfaction, the acoustic properties of hybrid vehicles are important. The vibro-acoustic behavior of internal combustion engines are nowadays well controlled, but the knowledge can’t be directly transferred to hybrid and electric vehicles without understanding the electric powertrains [3].

Firstly, the absence of masking noise from an ICE in a hybrid/electric vehicle can make the noise from other sources more annoying, such as rolling noise from the road. Even though the noise levels in electric vehicles generally are lower, new challenges occur with whining noise during acceleration and regenerative braking.

These noises are perceived both as low-frequency structure-borne noise and high-frequency airborne noise [4].

The electric powertrain consists of several components apart from the motor that emit noise. The cooling system emits airborne flow-noise, and the inverter emits high-frequency whining noise.

In a conventional ICE powered vehicle, the perceived feedback to the driver is based on engine speed and load. With an electric powertrain there is sometimes no clear connection between these two. It is important to find a good compromise between acoustic driver feedback and power demand to obtain good comfort [4].

## 2.4 Powertrain mounts

Powertrain mounts serve a number of functions for the overall vehicle. They maintain the powertrains position during inertia and torque loads, control motion to prevent interference with other components, plays role in handling due to the powertrains large mass and serves to isolate the vehicle from the powertrain vibrations [5]. The latter is of great importance for how the vehicle is perceived by the customer in terms of sound quality.

A powertrain has six degrees of freedom in its coordinate system (seen in figure 2.4-1). Firstly, there are three translational degrees of freedom, longitudinal, lateral and bounce, which are movements along the x, y and z-axis respectively. The remaining three are rotational; roll, pitch and yaw, around x, y and z [6].

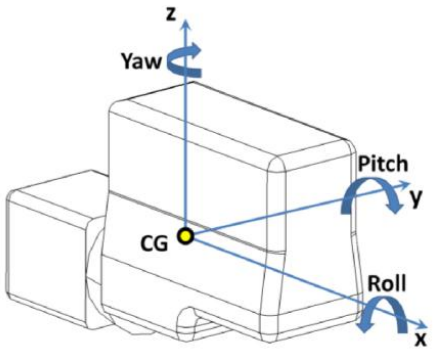


**Figure 2.4-1** Powertrain coordinate system, taken from [7]

There are currently three main approaches regarding powertrain mounting design layout (see figure 2.4-2). Each concept has specific advantages and disadvantages [7].

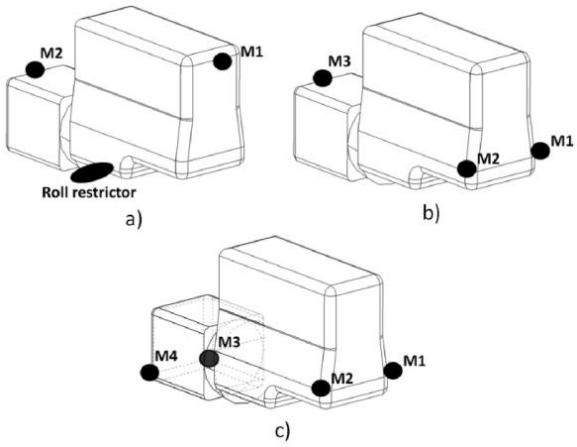


**Figure 2.4-2** Different designs, taken from [7]

- A 3-point torque roll axis layout with the advantage that forces and moments are well distributed between the three mounts. The torque roll axis is the axis around which only rotation occurs when a torque is applied on a free rigid body (see figure 2.4-3). Mount M1 and M2 carry the weight of the powertrain and restrict vertical, lateral and longitudinal displacement. The lower mount is used as a roll restrictor and controls the movement due to torque loads (see figure 2.4-2 a) ). This layout allows good tuning of characteristics but the mounts have to withstand high forces.

- The generic 3-point mounting layout (see figure 2.4-2 b) ), which benefits are low space requirement and cheap design. The downside is that all mounts are exposed to forces and moments, which decreases tuning possibilities.

- The 4-point mounting concept (presented in figure 2.4-2 c) ) has the advantage that lower mount forces can be achieved. The disadvantage is a more expensive and sensitive to mounting tolerances design.

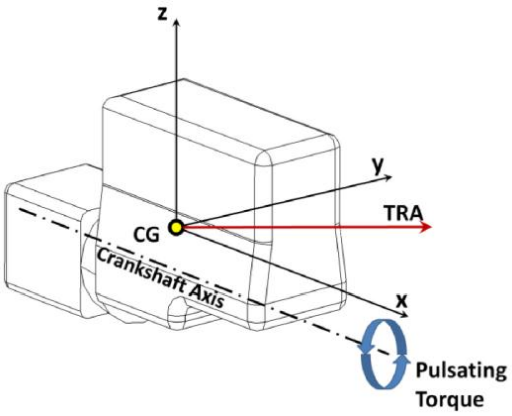


**Figure 2.4-3** Torque roll axis, taken from [7]

In order to achieve good vibrational control of the powertrain mounting system it is important to have the rigid-body modes decoupled as much as possible. Decoupling means that when the powertrain is excited, the response will occur in only one of the modes, which allows appropriate tuning of the system [7].

Depending on the vehicle type e.g. Sports- or Luxury car, the targets for the mounts may differ. The powertrain mounts in a sports car may be stiffer to increase feedback to the driver through vibrations and sounds, while the luxury car should give an overall more quiet experience [6].

## 2.5 Transfer path analysis

Transfer path analysis (TPA) is used to trace the flow of vibro-acoustic energy from an excitation source to a receiver. This is done by using measured or calculated transfer functions which describe the path from the source through the air- or structure to the receiver in combination with excitation forces at the source. The forces at the source are multiplied with the transfer function in each direction respectively and summed to a total noise- and/or vibration response at the receiver location according to equation (1) [8].

$$y_k = \sum_{i=1}^{n} NTF_{ik} * F_i + \sum_{j=1}^{p} NTF_{jk} * Q_j \quad [8]\ (1)$$

The left hand side of equation (1) is the total response at the receiver. The first term on the right hand side is the structural response which is the sum of each exciting force multiplied with the corresponding structural transfer function. The second term is the airborne response which is the sum of each airborne excitation multiplied with the corresponding airborne transfer function [8].

## 2.6 Blocked force approach

Consider two connected substructures e.g. a motor and a subframe (see figure 2.6-1). The motor acts as a source while the subframe acts as a receiver. If the internal forces from the source, i.e. the electric motor are unknown and not accessible, the blocked force approach can be applied to obtain them at the interface [9].

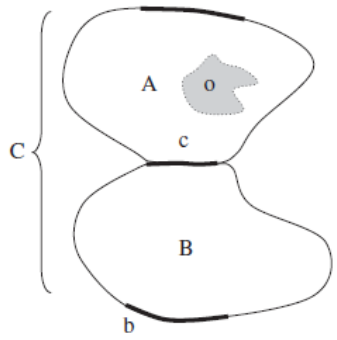


**Figure 2.6-1** Coupled structures, taken from [9]

To use the blocked force approach in-situ, i.e. with source and receiver connected, a two-stage measurement procedure is required. Firstly, the operational velocity is measured at arbitrary points on the receiver structure. Thereafter the mobility matrix for the coupled system is measured at the same points to solve equation (2) [9].

$$\boldsymbol{v_b} = \boldsymbol{Y}^T_{\boldsymbol{C,cb}} \boldsymbol{f_{bl}} \text{ [9]} \qquad (2)$$

The left hand side of equation (2) is the operational velocity vector. The first term on the right hand side is the mobility matrix for the coupled system. It contains the transfer function for each degree of freedom. The second term of the right hand side is the blocked force vector. This equation is then solved for each frequency.

## 2.7 Volvo V60 Plug-in hybrid

The Volvo V60 D6 AWD Plug-In hybrid is a parallel hybrid equipped with two powertrains. The front wheels are powered by a 2.4l diesel engine producing 215 hp. The rear wheels are powered by an electric motor which produces 68 hp. The rear driveline assembly is called ERAD (Electric Rear Axle Drive). The vehicle can be driven purely electric for 50km and fulfills the environmental classification EURO 5b+ [10].

The ERAD consists of an electric motor combined with a fixed gear planetary transmission and clutch (see figure 2.7-1). The electric motor is a water cooled Magna 3-phase AC PMSM with a rotor diameter of 180 mm. Its peak output is 50 kW for 15 seconds and 20 kW continuously. The maximum rotor speed is 12000 rpm and peak torque is 200 Nm. The ERAD weighs 49.7 kg including high voltage cables and oil.

**Figure 2.7-1** ERAD cross section cut. Courtesy of Magna Powertrain.

The transmission is a coaxial design with a planetary gear set and an integrated open differential. It has 200 Nm input torque capacity and its fixed gear ratio is 9.17:1, meaning that the electric motor speed is 9.17 times higher than the drive shaft output. A clutch is used to disconnect the electric motor from the transmission, consisting of a worm gear connected to a dog clutch (shown in figure 2.7-2).

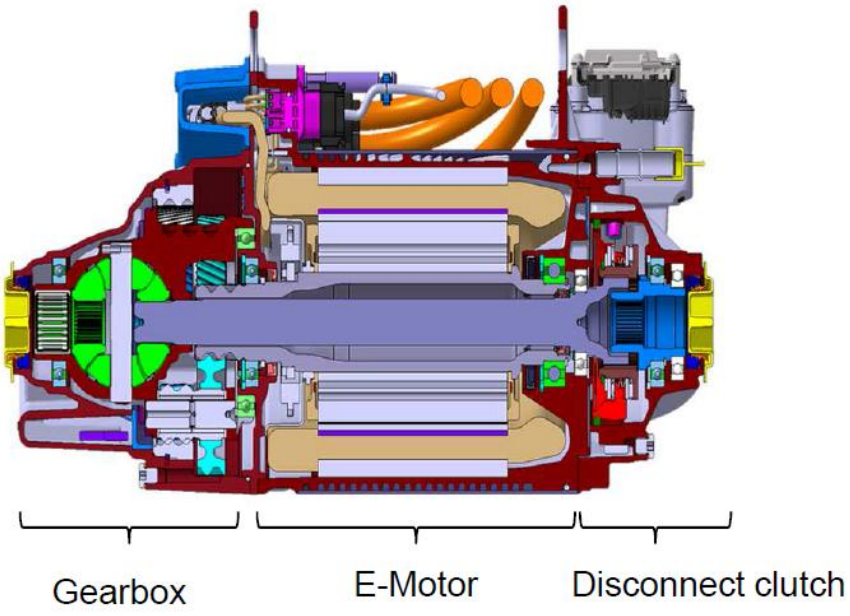


**Figure 2.7-2** ERAD section view. Courtesy of Magna Powertrain.

# 3 Method

*This chapter describes the work process.*

## 3.1 Operational measurements

The operational measurements and data extraction performed in the thesis were done in collaboration with David Lennström. The sound recordings were made with four microphones located at the outer ear position on each seat inside the interior of a Volvo V60 (3.1-1). Furthermore, eight triaxial accelerometers were glued to the rear subframe (see figure 3.1-2). These were used to record acceleration in x, y and z respectively during driving. Additionally, CAN-data was recorded from the vehicle containing ERAD rpm. A LMS frontend was used together with the LMS Test.Lab software to collect data. The measurement setup is found in appendix A.

**Figure 3.1-1** Microphones at outer ear position in V60 rear seat

The sound- and time-data files were recorded on dry road during slow acceleration from 0-20 km/h upwards a hill. This driving-case was chosen because the tram-noise was clearly audible at these conditions.

**Figure 3.1-2** Rear suspension with accelerometers glued at arbitrary points and aluminum bosses glued to mounting points

## 3.2 Data extraction

The recorded data was extracted using the LMS Test.Lab software. The three prominent engine orders 10, 30 and 90 can be seen in figure 3.2-1. The electric motor has five pole pairs with orders that correspond to multiples of them, e.g. order 10, 15, 20 etc. Engine orders are calculated with equation (3) were *n* is the engine order number.

$$frequency = \frac{rpm}{60} * n \tag{3}$$

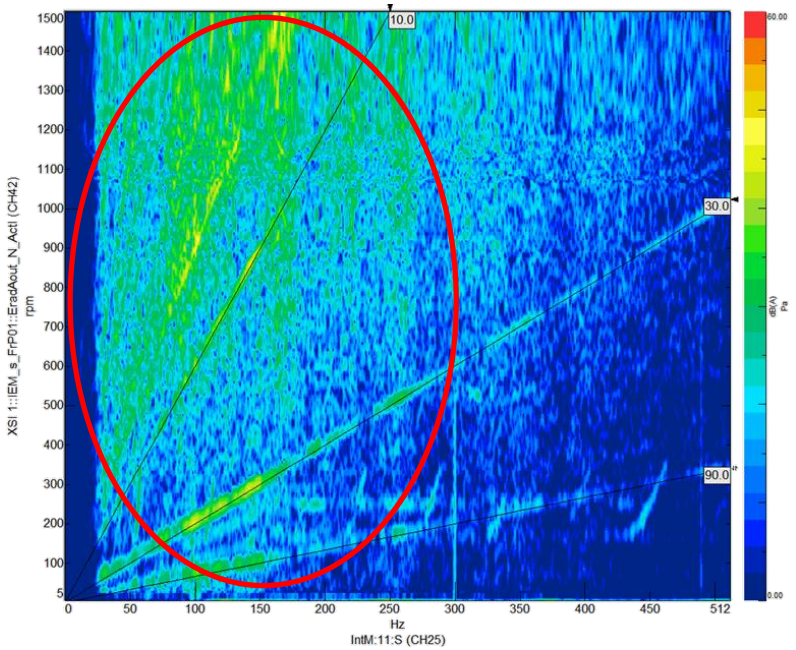


**Figure 3.2-1** Engine orders 10, 30 and 90 recorded during driving where the problem area is marked in red

The frequencies were the noise occurs are seen in figure 3.2-1 and are from about 50 to 300 Hz.

### 3.3 NTF-measurements

In order to find which transfer paths that are the largest contributors to the interior SPL a transfer path analysis was performed (see chapter 2.5). It consists of measuring frequency response functions between each of the ERAD mounting points, the subframe and the interior microphones in each direction respectively (numbered as seen in figure 3.3-1). These frequency response functions are then multiplied with the calculated forces acting at the mounting points and the interior SPL spectra is reconstructed as a sum of them. The largest contributors can then be identified. This was made for engine order 10, 30 and 90 but this chapter only shows the results for order 10. The remaining orders can be found in appendix B.

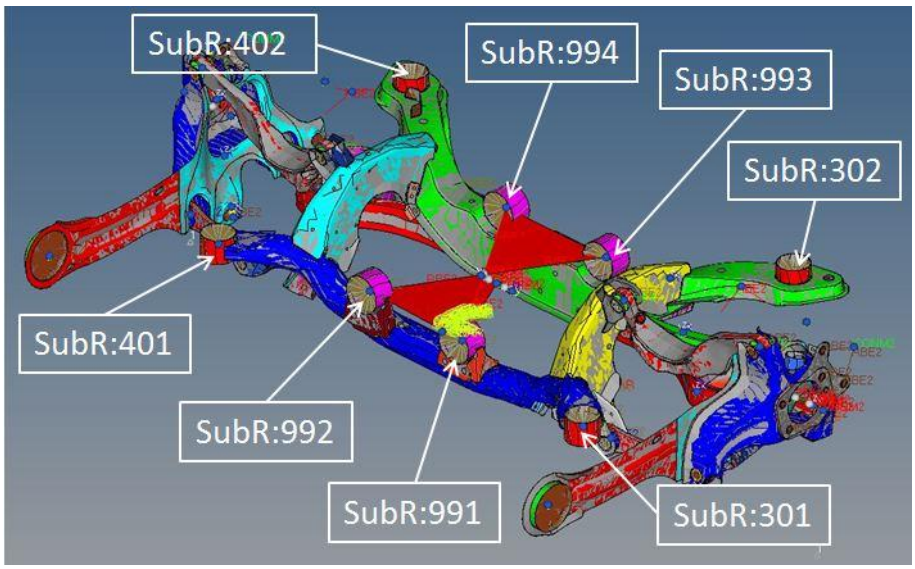


**Figure 3.3-1** Rear suspension CAE model with Volvo nomenclature

The NTF-measurements were performed with the same measurement setup as the operational setup. Instead of driving the vehicle, it was placed on a 4-post car lift. The four ERAD mounting points (see figure 3.1-2) were excited using a hammer fitted with a force transducer. A cubic aluminum boss (approx. 10 by 10 mm) was glued to each mounting screw to easier excite the three directions x, y and z respectively (seen figure 3.1-2). Two different hammers and four different tips were evaluated to obtain the best possible coherence (how well the response can be described by the measured transfer functions). Each ERAD mounting point was excited in the x, y and z direction while the responses at the interior microphones and at the accelerometers on the subframe were recorded. Simultaneously the hammer input force was recorded using the LMS frontend and software. Frequency response functions from the ERAD mounting points to the passenger microphone are shown in figure 3.3-2. The transfer functions are higher in the z-direction than the x- and y-directions for all four points.

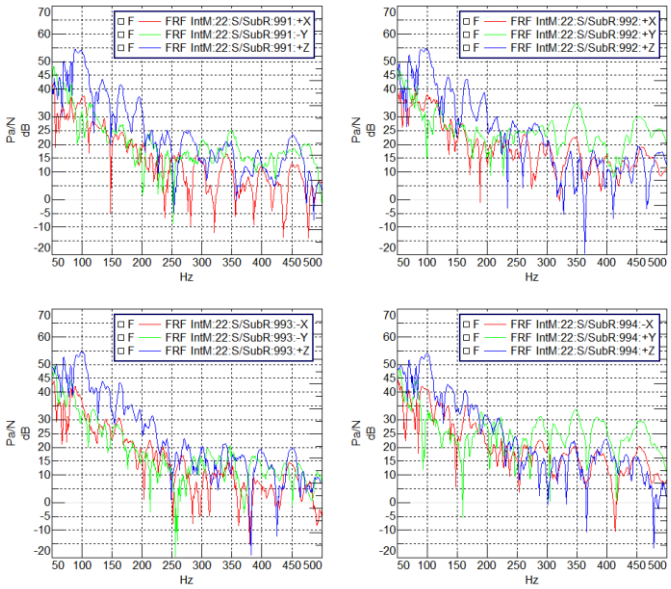


**Figure 3.3-2** NTFs order 10

The best coherence was obtained using a large hammer equipped with a plastic tip (see figure 3.3-3). The coherence is high up to 200 Hz but is thereafter decreasing for all directions and engine orders (see figure 3.3-3 and appendix B).

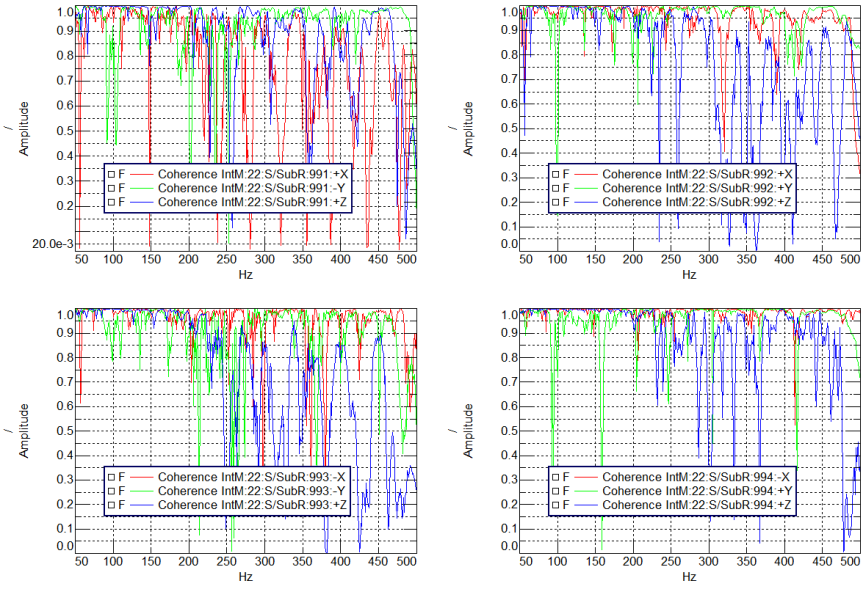


**Figure 3.3-3** Coherence between passenger microphone and ERAD mounting points from NTF measurement

The calculated forces at the ERAD mounting points are shown in figure 3.3-4. Similar levels are obtained in x, y and z. Forces for order 30 and 90 are found in appendix B.

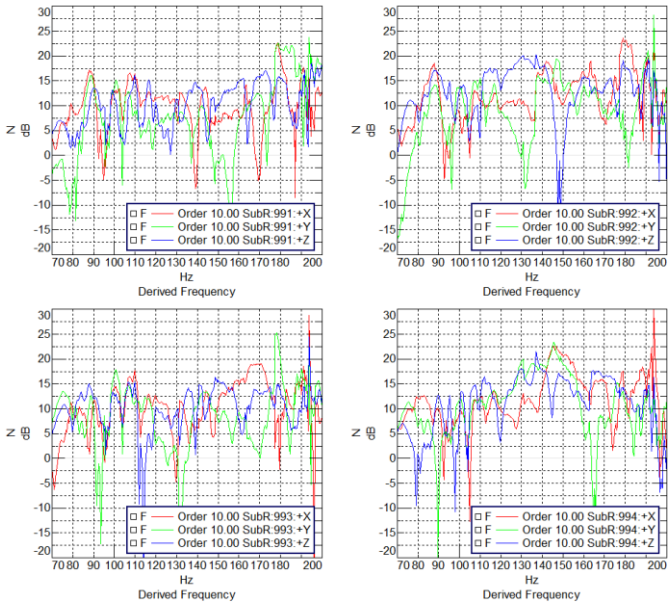


**Figure 3.3-4** Engine order 10 calculated forces at the mounting points

The measured response (in green) is compared to the reconstructed response (in red) for engine order 10 and is shown in figure 3.3-5. Poor signal to noise ratio is seen below 70- and above 200 Hz. This is somewhat better for order 30 and 90 where the SNR is ok up to 150 Hz.

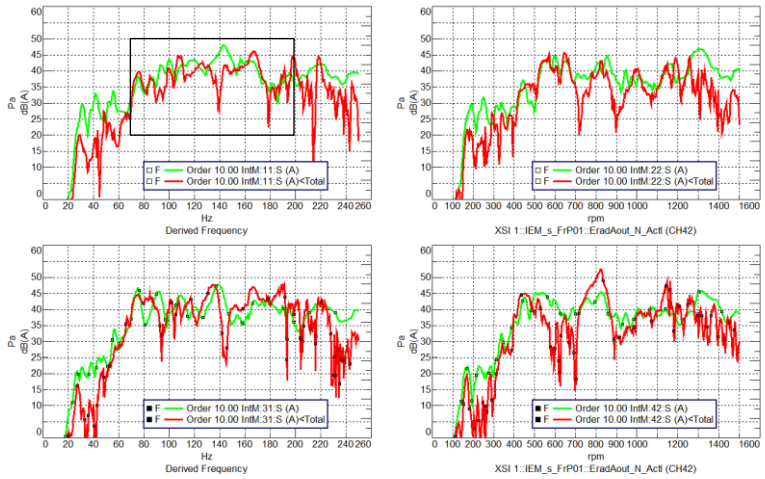


**Figure 3.3-5** Order 10 measured vs. reconstructed response at microphones

The largest contributors to the interior SPL are the z-directions from the four ERAD mounting points. Figure 3.3-6 shows engine order 10 and remaining orders show similar results and are found in appendix B. This is probably caused by the layout of the existing installation were the torque ripple is transferred mostly through z while the vehicle is more sensitive in z (see figure 3.3-2).

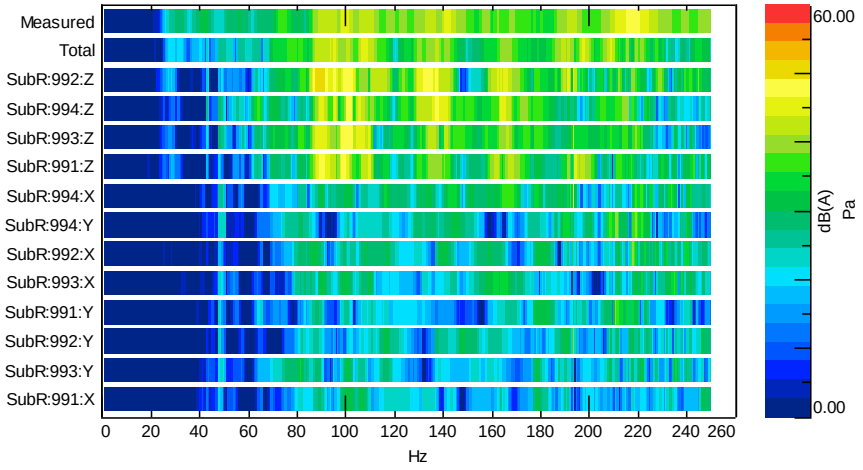


**Figure 3.3-6** SPL contributors for engine order 10

## 3.4 Existing installation

The existing ERAD installation is seen in figure 3.4-1. The rear bushing mounts are carried over from a V60 AWD rear differential while the two front mounts are ERAD specific.

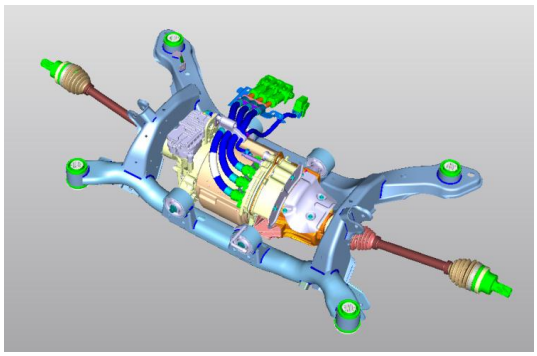

**Figure 3.4-1** Rear subframe with ERAD and driveshafts

The four bushings are equal and seen in figure 3.4-2. Their dynamic stiffness in x, y and z is seen in table 3.4-1.

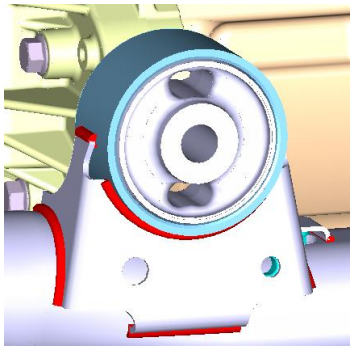

**Figure 3.4-2** ERAD rear left bushing

**Table 3.4-1** ERAD bushing stiffness at 100 Hz with 0.025mm amplitude

| | X | Y | Z |
|---|---|---|---|
| N/mm | 235 | 1390 | 850 |

Using Volvos nomenclature, the subframe- and ERAD mounts are numbered as seen in figure 3.3-1. Coordinates for the ERAD bushing positions given in the vehicle coordinate system are seen in table 3.4-2. The center of gravity for the ERAD is positioned according to table 3.4-3.

**Table 3.4-2** ERAD bushing coordinates

| | X [mm] | Y [mm] | Z [mm] |
|---|---|---|---|
| Subr:991 | 4372.5 | -86 | 413.5 |
| Subr:992 | 4372.5 | 146 | 420.5 |
| Subr:993 | 4695 | -125.4 | 469.4 |
| Subr:994 | 4695 | 125.4 | 469.4 |

**Table 3.4-3** ERAD center of gravity given in the vehicle coordinate system

| X [mm] | Y [mm] | Z [mm] |
|---|---|---|
| 4537 | 23.5 | 438 |

## 3.5 Concept generation

After studying electric motor installations of some competitors, such as Tesla Model S, Tesla Roadster and Citroën DS4, five concepts were generated in order to evaluate how different installation layouts affect the sound level at the driver's ear. The concepts were designed based on the principles mentioned in chapter 2.4. The following limitations were applied;

- Keep the inner base structure of the rear subframe and the ERAD (see figure 3.4-1), meaning that the concept should be able to implement in an existing vehicle if wanted.

- Surrounding components, such as the exhaust pipe, cables and cooling equipment is assumed to be able to move if needed.

The concepts are described in chapter 3.5.1 through 3.5.5, were the inner subframe structure is shown in dark blue, the ERAD is represented in grey and the bushings (with their corresponding directions) between them are represented as boxes and circles.

### *3.5.1 Concept 1*

Concept 1 features three mounts. The front mount is located in the middle of the front subframe tube while the two other mounts are located in the rear corners and connected to the side- and rear tubes. The front mount is in line with (z-direction) the front tube and both the rear mounts are slightly higher than the rear tube.

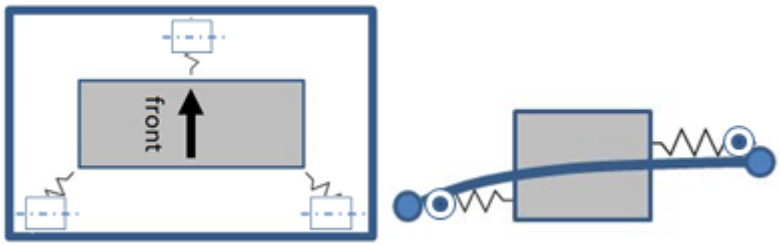


**Figure 3.5-1** Concept 1 layout

### *3.5.2 Concept 2*

Concept 2 also features three mounts (approach from figure 2.4-2 b) ). This concept has two mounts on the left side, located in the front- and rear corner. The right mount is located in the middle (x-direction) between the front- and rear subframe tube. The height difference between the left mounts is decreased, which has shifted up the front mount compared to concept 1. The right mount is placed at CoG height for the ERAD which aim to decrease the forces in z-direction when torque is applied.

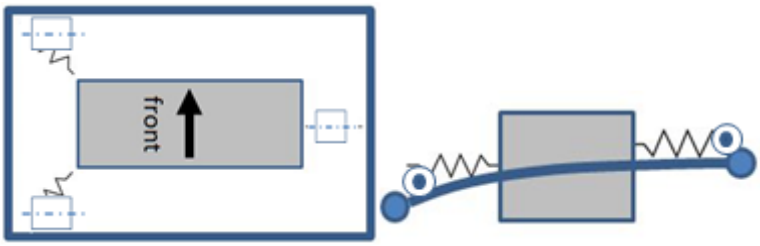


**Figure 3.5-2** Concept 2 layout

### *3.5.3 Concept 3*

Concept three consists of four mounts (approach from figure 2.4-2 c) ), which are located at the front- and rear corners of the inner subframe structure. The two front mounts are placed slightly higher than the front subframe tube. The rear mounts are also moved slightly higher than the rear subframe tube.

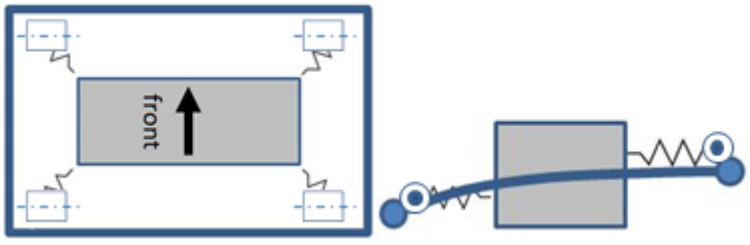


**Figure 3.5-3** Concept 3 layout

### *3.5.4 Concept 4*

Concept 4 is also features three mounts (see figure 2.4-2, b) ), but it differs from concept 1 and 2. It has one front and one rear mount located in the middle (y-direction). The third mount is placed at the right side and is located at CoG-height (z-dir).

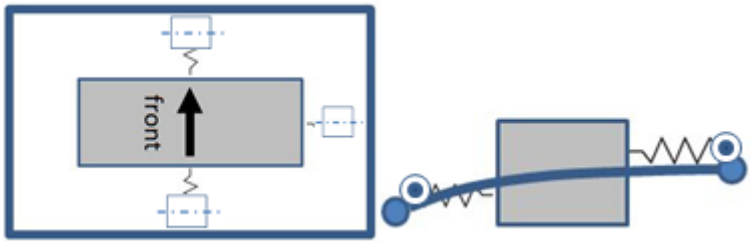


**Figure 3.5-4** Concept 4 layout

### *3.5.5 Concept 5*

Concept 5 is based on the approach seen in figure 2.4-2 a) with two mounts placed at the sides and one lower link. The mounts at the sides are placed at the same x and z coordinate as the ERAD CoG to minimize torque forces. The lower link is fitted to the rear subframe tube and connects it to the ERAD through a bushing.

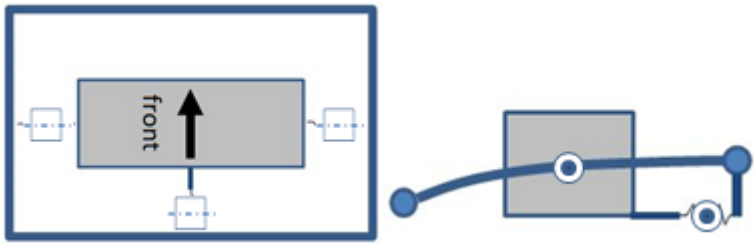


**Figure 3.5-5** Concept 5 layout

## 3.6 CAE Analysis and concept evaluation

### *3.6.1 Model setup*

Altair Hyperworks with the NVH-Director plugin was used to analyze and evaluate the concepts and the existing installation. The software was used during the whole process, from building concept layouts through analysis and finally data extraction. A V60 complete vehicle model (seen in figure 3.6-1) was used. The model is reduced with the Craig-Bampton method to reduce calculation time.

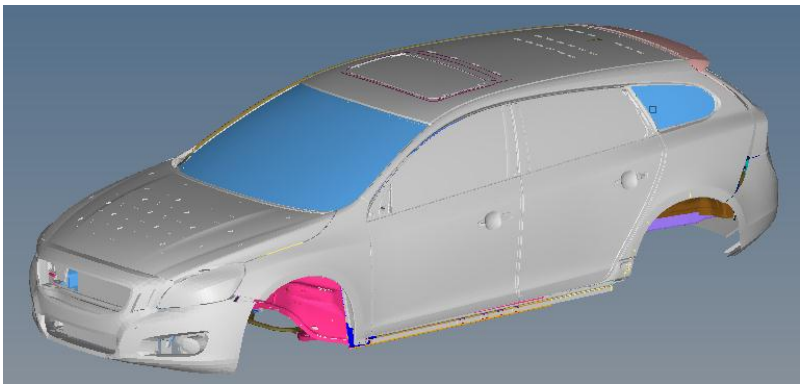

**Figure 3.6-1** Complete vehicle model

The vehicle coordinate system is denoted as the following; x-axis pointing rearwards, y-axis pointing right and z-axis pointing upwards.

The rear suspension model including the ERAD is shown in figure 3.3-1. Suspension components are modeled as plot elements, drive shafts as CBAR elements and the ERAD is modeled as a rigid body with weight and inertia in x, y and z as described in table 3.6-1.

**Table 3.6-1** ERAD weight and inertia

| Weight | $I_{xx}$ $[kgm^2]$ | $I_{yy}$ $[kgm^2]$ | $I_{zz}$ $[kgm^2]$ |
|---|---|---|---|
| 44.83kg | 0,65621 | 0,63897 | 0,21684 |

Bushings are modeled as CBUSH elements with stiffness in x, y and z directions and a small mass; 1e-6 ton.

### *3.6.2 Load case*

To understand how the torque ripple acting from the electric motor affect the interior sound pressure level, a general frequency response load case is defined. The load case calculates the responses in chosen points when a load is applied on an arbitrary point on the structure. These force responses are then multiplied with NTFs measured on a vehicle with production status to obtain the sound pressure level at the driver's ear. The frequency spectrum was chosen in a way that it covers most of the frequencies were tram noise is present, i.e. a spectrum from 1 to 150 Hz.

Usually when vehicles are equipped with ICEs, the gas forces acting on the pistons are calculated for different RPMs and applied on the crank shaft in the CAE-model with a frequency-dependent load table. In this case, the forces produced by the electric motor aren't available due to the difficulty in modeling electro-magnetic forces accurately. Therefore the calculated forces (from chapter 3.3) are applied at the existing mounting points. This response is then compared with a unit load applied at

the ERAD center of gravity which is tuned to create a similar sound pressure level at IntM1. Several simulations were performed with the result that 1 Nm conforms approximately to the measured forces (see figure 3.6-3). This is done to be able to compare the concept layouts were the forces at the mounting points are unknown.

Table 3.6-2 shows the other vehicle component status. It puts the vehicle in idle with unlocked springs, brakes and drive shafts. The shock absorbers are unlocked while the transmission lockup spring is disengaged.

**Table 3.6-2** Component status

| **Component** | **Status** |
|---|---|
| Front brakes | Off |
| Rear brakes | Off |
| Front shock absorbers | Unlocked |
| Rear shock absorbers | Unlocked |
| Front drive shafts | Drive |
| Rear drive shafts | Drive |
| Lockup spring | Disengaged |
| Engine mounts | Idle preload |

The response points used in the model are the four points were the rear subframe is mounted onto the vehicle body (301, 302, 401 and 402 seen in figure 3.3-1). The responses are calculated on the body side, meaning that the forces pass both the ERAD- and subframe bushings.

### *3.6.3 Existing installation analysis*

The installation used in existing vehicles is analyzed with the load case described in 3.6.2. The interior sound pressure level at IntMic1 with blocked forces applied is seen in figure 3.6-2.

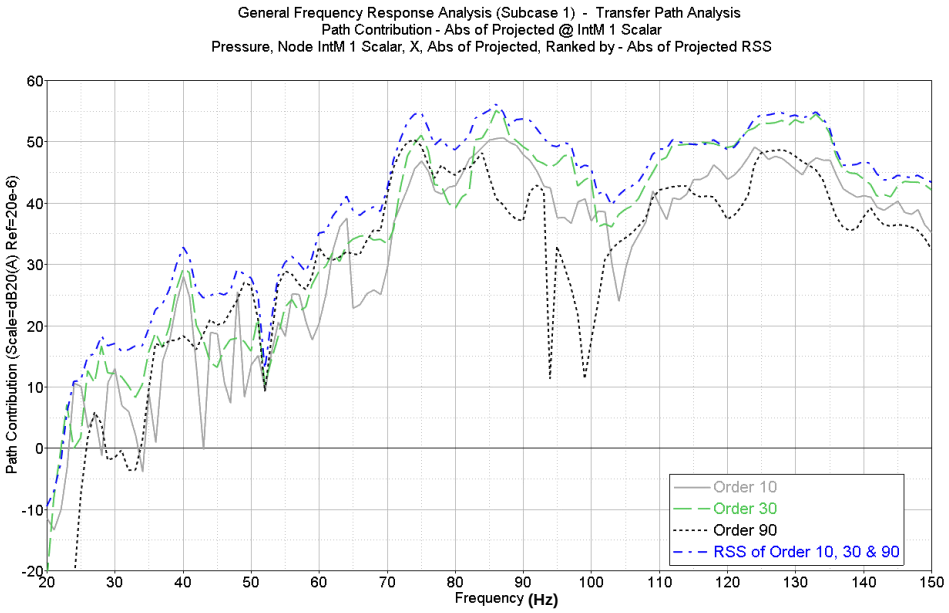


**Figure 3.6-2** SPL at IntM1 for order 10, 30, 90 with existing installation

The unit load described in 3.6.2 compared with blocked force RSS is seen in figure 3.6-4. The unit load under-predicts between 30-40 Hz and 70-100 Hz. This is probably due to a somewhat higher (but unknown) excitation level at these frequencies.

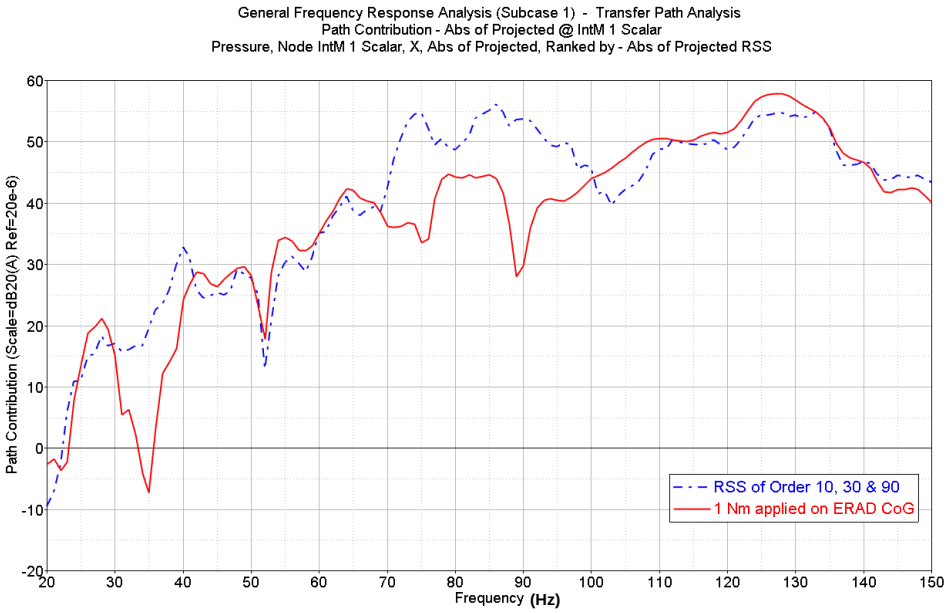


**Figure 3.6-3** SPL at IntM1 comparison, order RSS vs. unit load applied on existing installation

### *3.6.4 Concept modeling*

The new mounting positions were modeled with rigid body elements placed on the subframe mesh (seen in figure 3.6-4). ERAD mounting nodes were changed to coincide with the new nodes on the subframe side. The connections between ERAD and subframe were modeled with bushing-connectors with stiffness in x, y, and z directions calculated using equation (4). The right hand side mount from concept 2 is seen in figure 3.6-4.

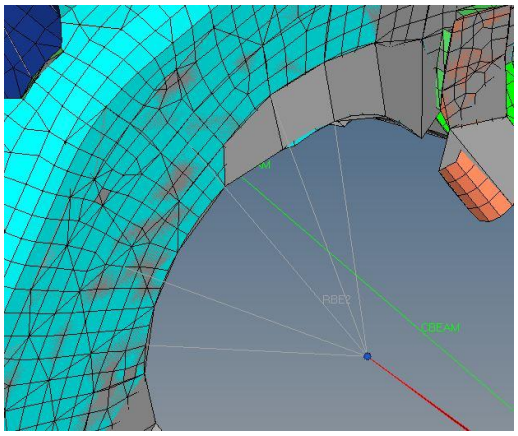

**Figure 3.6-4** Concept 2 right mount in CAE model

To compare different concepts, the total bushing stiffness was kept the same as the existing installation in each direction. This was done by dividing the total stiffness in each direction with the number of mounting positions for the current concept according to equation (4).

$$k_{i=x,y,z}^{concept} = \frac{1}{n_{concept}} \sum_{j=1}^{4} k_{i,j} \qquad (4)$$

Were $k_{i=x,y,z}^{concept}$ is the new stiffness, $k_{i,j}$ is the existing stiffness and $n_{concept}$ is the number of mounts for the concept layout.

The bushing stiffness for two, three- and four-point installation concepts are given in table 3.6-3.

**Table 3.6-3** Concept bushing stiffness given by number of mounting points

| | X [N/mm] | Y [N/mm] | Z [N/mm] |
|---|---|---|---|
| Two point | 470 | 2780 | 1700 |
| Three point | 313 | 1853 | 1133 |
| Four point | 235 | 1390 | 850 |

The five concepts modeled in Hyperworks are shown in figure 3.6-5 to 3.6-9. Their corresponding mounting point coordinates are seen in table 3.6-4 to 3.6-8.

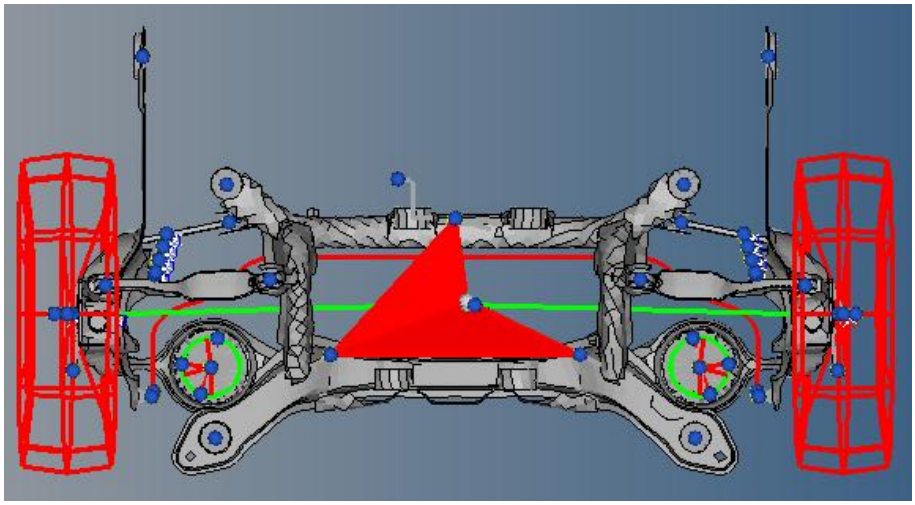

**Figure 3.6-5** Concept 1 upper view

**Table 3.6-4** Concept 1 mounting point coordinates

| | X [mm] | Y [mm] | Z [mm] |
|---|---|---|---|
| Front mount | 4372.5 | 0 | 400 |
| Left mount | 4645 | -250 | 520 |
| Right mount | 4645 | 250 | 520 |

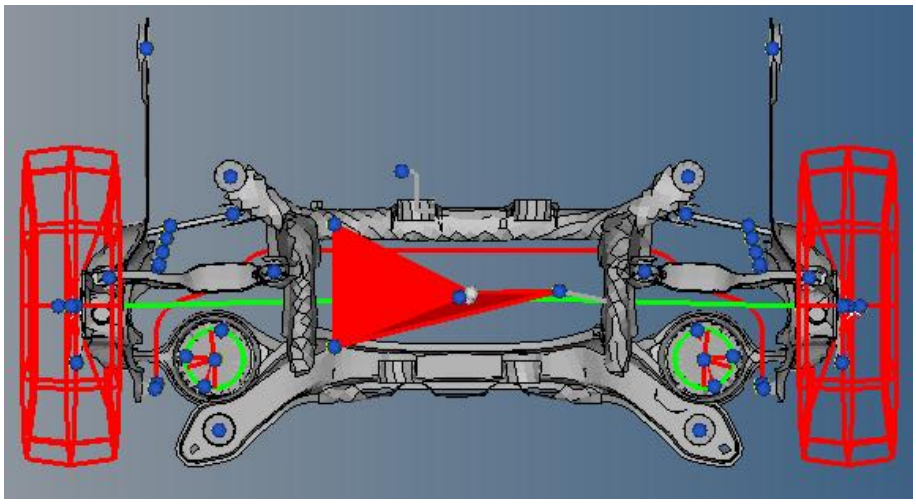

**Figure 3.6-6** Concept 2 upper view

**Table 3.6-5** Concept 2 mounting point coordinates

| | X [mm] | Y [mm] | Z [mm] |
|---|---|---|---|
| Front left mount | 4400 | -250 | 413 |
| Rear left mount | 4645 | -250 | 520 |
| Right mount | 4534 | 200 | 500 |

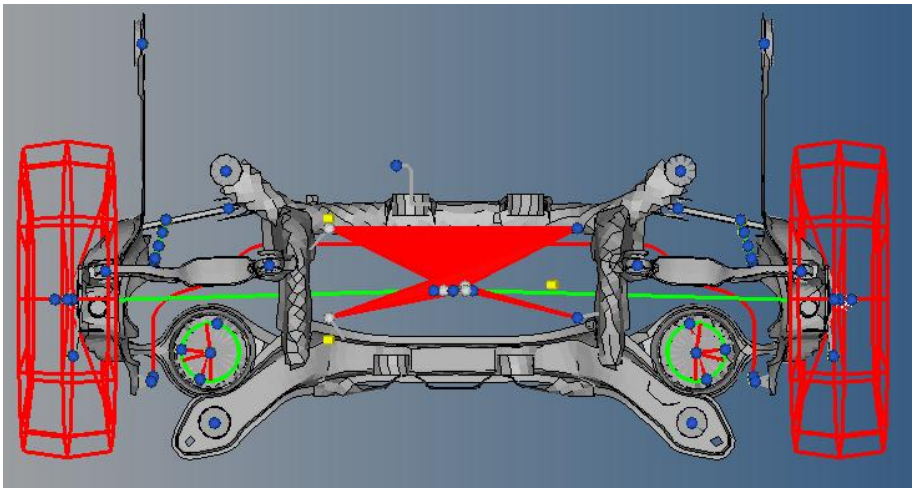

**Figure 3.6-7** Concept 3 upper view

**Table 3.6-6** Concept 3 mounting point coordinates

| | X [mm] | Y [mm] | Z [mm] |
|---|---|---|---|
| Front left mount | 4420 | -250 | 430 |
| Front right mount | 4420 | 250 | 430 |
| Rear left mount | 4600 | -250 | 460 |
| Rear right mount | 4600 | 250 | 460 |

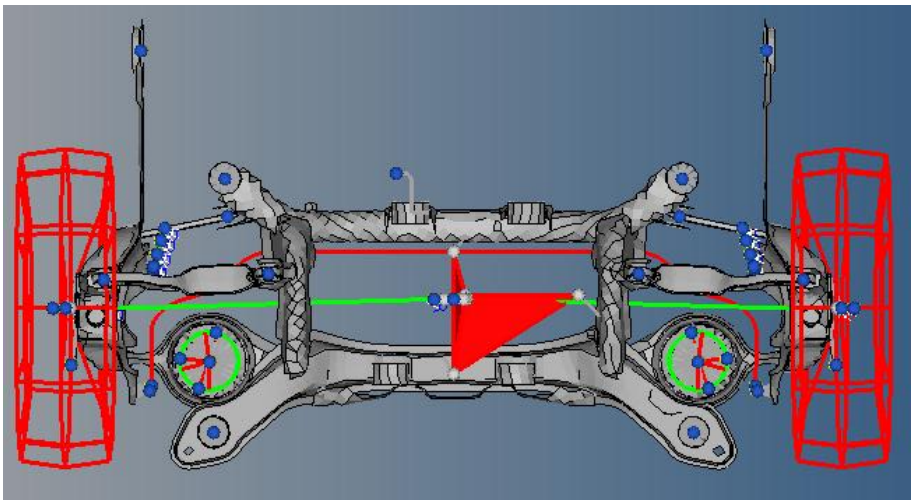

**Figure 3.6-8** Concept 4 upper view

**Table 3.6-7** Concept 4 mounting point coordinates

| | X [mm] | Y [mm] | Z [mm] |
|---|---|---|---|
| Front mount | 4450 | 0 | 340 |
| Rear mount | 4695 | 0 | 469 |
| Right mount | 4537 | 250 | 438 |

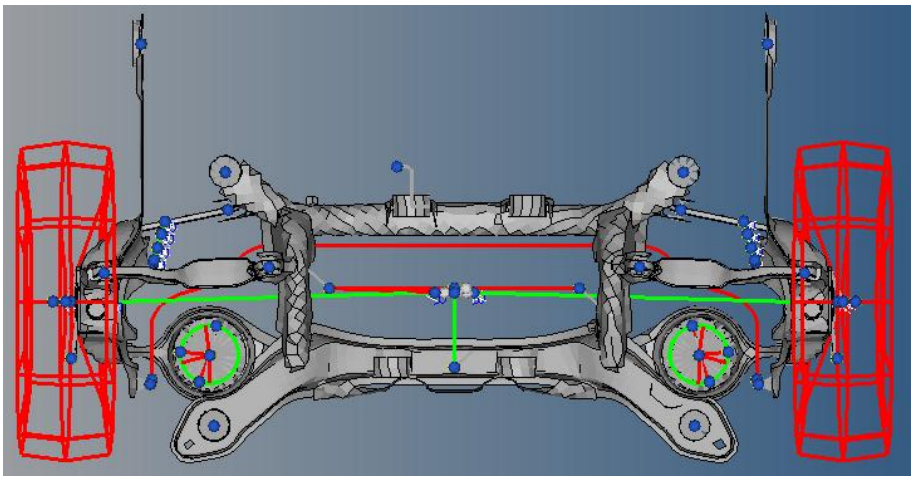

**Figure 3.6-9** Concept 5 upper view

**Table 3.6-8** Concept 5 mounting point coordinates

| | X [mm] | Y [mm] | Z [mm] |
|---|---|---|---|
| Left mount | 4537 | -250 | 438 |
| Right mount | 4537 | 250 | 438 |
| Torque rod front mount | 4600 | 0 | 330 |
| Torque rod rear mount | 4684 | 0 | 363 |

### *3.6.5 Concept comparison*

The load case described in 3.6.2 was applied to all five concepts. The sound pressure level at IntM1 is seen in figure 3.6-10.

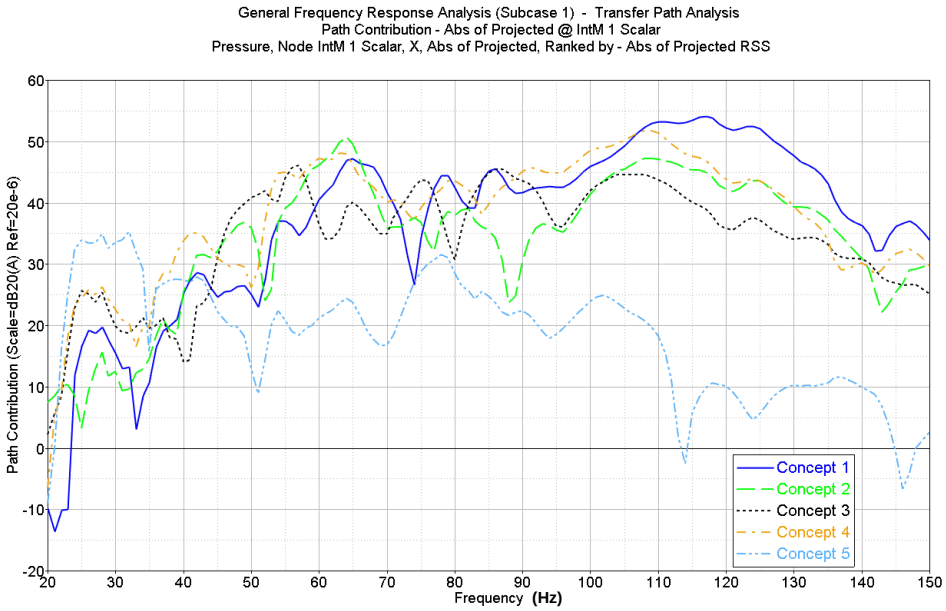


**Figure 3.6-10** IntM1 SPL comparisons for concept 1 to 5

Concept 5 was chosen for further development because it shows a lower SPL than the other concepts above 43 Hz. A SPL comparison between the existing installation and Concept 5 is shown in figure 3.6-11.

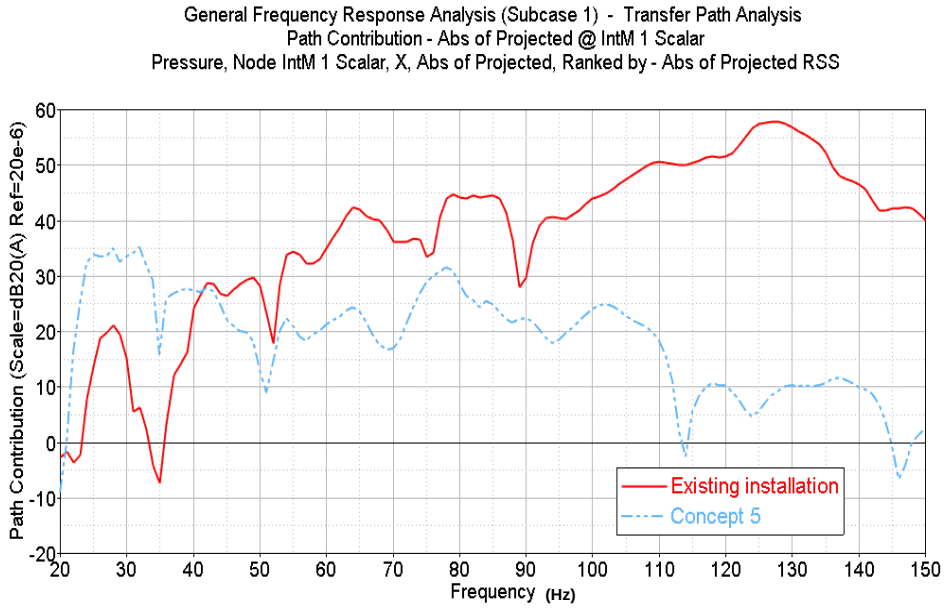


**Figure 3.6-11** IntM1 SPL comparison; concept 5 vs. existing installation

## 3.7 Catia design process

### *3.7.1 Design space study*

The design process started with a detailed study of the complete rear suspension in a Teamcenter Visualization Mockup environment. It was made to identify design space were a new mounting layout could fit. The complete rear suspension is shown again in figure 3.7-1.

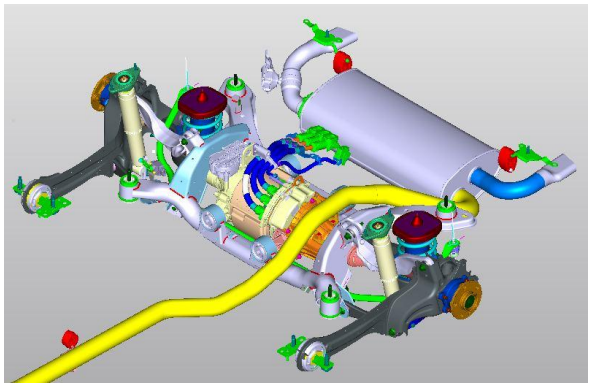

**Figure 3.7-1** Complete rear suspension in Teamcenter Visualization Mockup

The outcome of the study is listed below:

- Mounting brackets (were the bushings are placed on the existing installation) have to be removed to give access to the ERAD stator mounts
- Exhaust pipe needs to be moved (or removed) to give room for the left side mount
- The side mounts have to be positioned higher than CoG-height due to drive shaft position
- The lower torque rod needs a compact design with regard to ground clearance

### *3.7.2 Design*

The outcome of the design space study resulted in a first sketch of a possible installation. It consists of a structure that is mounted onto the existing stator mounting points. It is seen in figure 3.7-2.

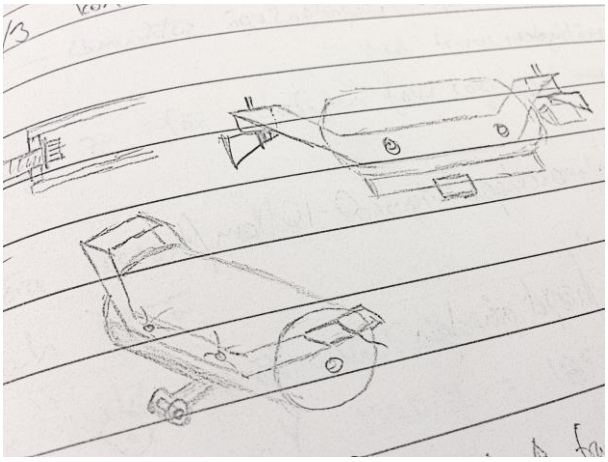

**Figure 3.7-2** First sketch of surrounding ERAD structure

Sketches of the lower torque rod and side mounts are seen in figure 3.7-3. To achieve a compact design with a minor effect on ground clearance, the rear torque rod bushing is placed inside the subframe tube. The front bushing is intended to be positioned on brackets that are welded onto the stator housing. Based on the sketch, the concept was designed in Catia V5. The surrounding structure and the lower torque rod are seen in figure 3.7-4. The surrounding structure is intended to be manufactured of 5mm water- or laser cut steel plates which are bent and welded at appropriate points. The lower torque rod is intended to be manufactured of aluminum with appropriate properties.

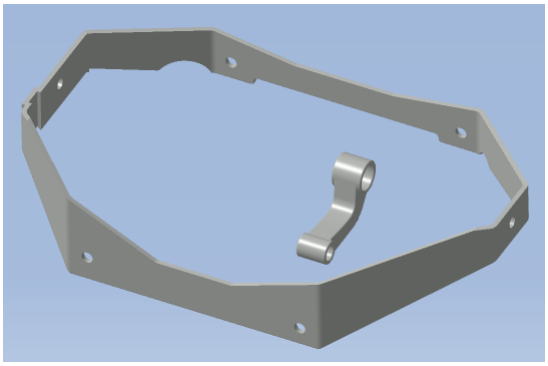

**Figure 3.7-3** Surrounding structure and lower torque rod

The side mounts are shown in figure 3.7-5. The 4mm brackets (in blue) are thought to be welded to the subframe side tubes. The bushing housings (in orange) are bolted to the brackets with two M10x30 each. The others are M12x45. The bushing direction is changed compared to the sketch (figure 3.7-2) to allow better rotation around the y-axis.

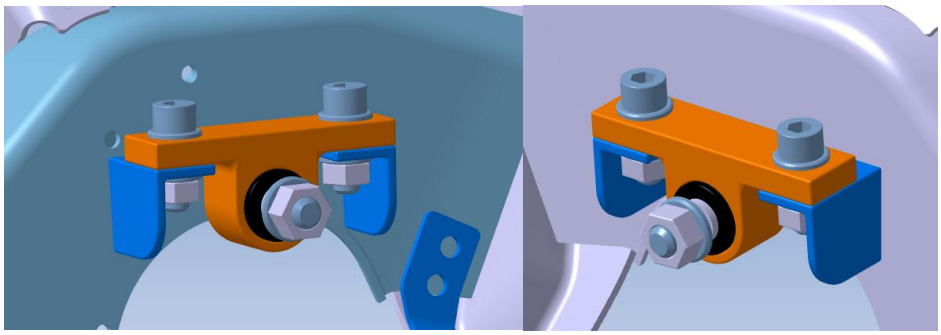

**Figure 3.7-4** Right and left side mount assembly

Figure 3.7-6 shows the torque rod and its corresponding brackets. The front brackets (in red) are intended to be welded onto the ERAD stator housing which is made of aluminum. Therefore the front brackets are slightly thicker (5mm) compared to the rears which are made of 4mm steel. The rear brackets (in blue) are placed inside the rear subframe tube. Bolt sizes are M12x70.

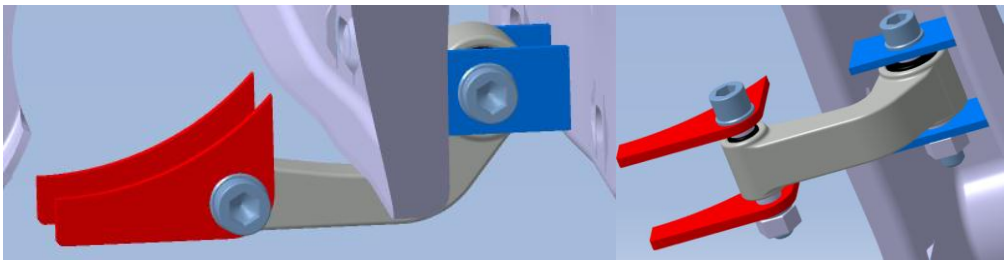

**Figure 3.7-5** Lower torque rod with corresponding bolts and brackets

An overview of the assembled concept design with and without ERAD is shown in figure 3.7-7. Further views are found in appendix C.

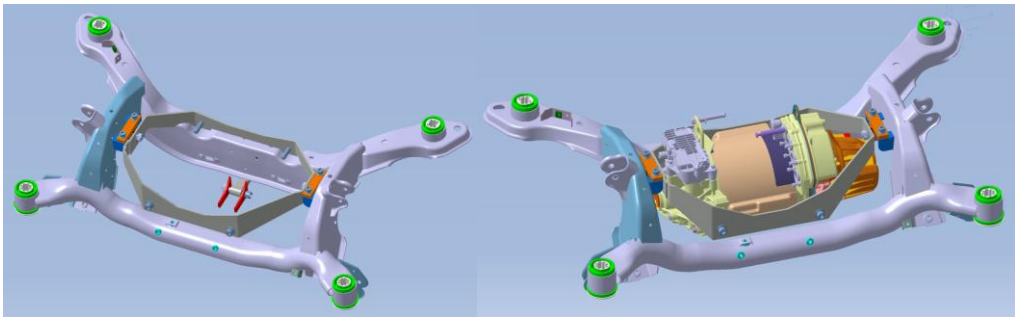

**Figure 3.7-6** Concept design with and without ERAD

The updated mounting positions for the concept layout are seen in table 3.7-1. Both side mounts are moved higher in z to avoid drive shaft interference while the torque rod coordinates are the same as the initial concept.

**Table 3.7-1** Final mounting position coordinates

| | X [mm] | Y [mm] | Z [mm] |
|---|---|---|---|
| Left mount | 4537 | -250 | 500 |
| Right mount | 4537 | 250 | 500 |
| Front torque rod point | 4600 | 0 | 330 |
| Rear torque rod point | 4684 | 0 | 363 |

## 3.8 Bang oscillation simulation

To further evaluate the behavior of the installation concept and compare it to the existing installation, a multi body dynamics model in ADAMS was used (see figure 3.8-1). The study was performed to analyze bushing deflections at high load conditions to avoid interference between components. The bushing stiffness used in table 3.6-3 was not yet validated for avoiding interference for the concept layout.

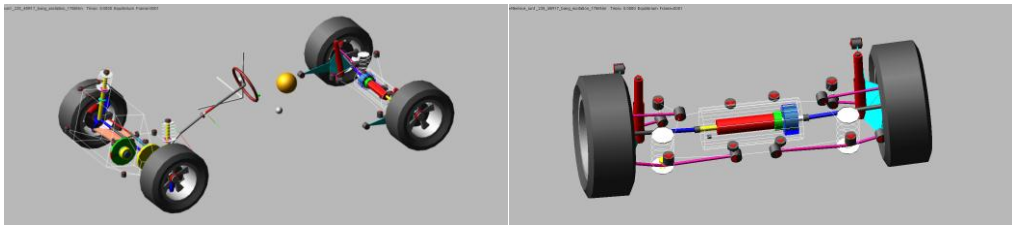

**Figure 3.8-1** Overview of the ADAMS model

The model of a V60 Plug-In hybrid was excited with a “Bang Oscillation” load case. Bang oscillation implies that the vehicle is given an initial velocity (100 km/h) on a slippery road (μ=0.2). After one second, full brake pressure is applied to the calipers, causing the anti-lock brake system to engage. The total drive shaft torque for the existing installation is shown in figure 3.8-2.

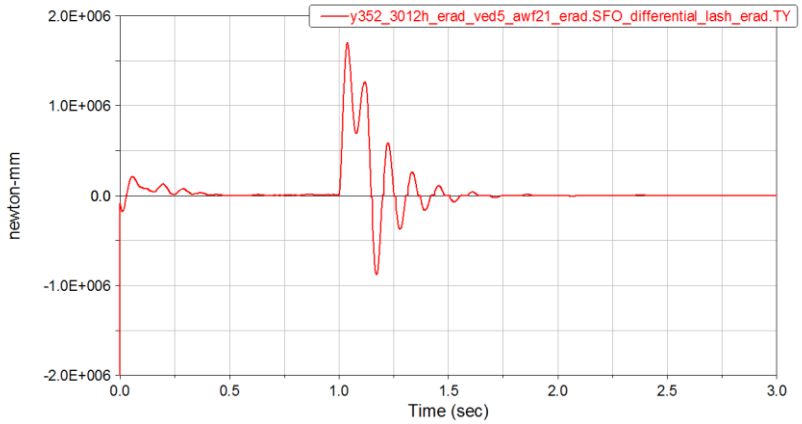


**Figure 3.8-2** Rear drive shaft torque excitation (existing installation)

The displacement for all ERAD mounts were recorded and are found in appendix D. Z-direction showed the largest displacement and is seen in figures 3.8-3 and 3.8-4.

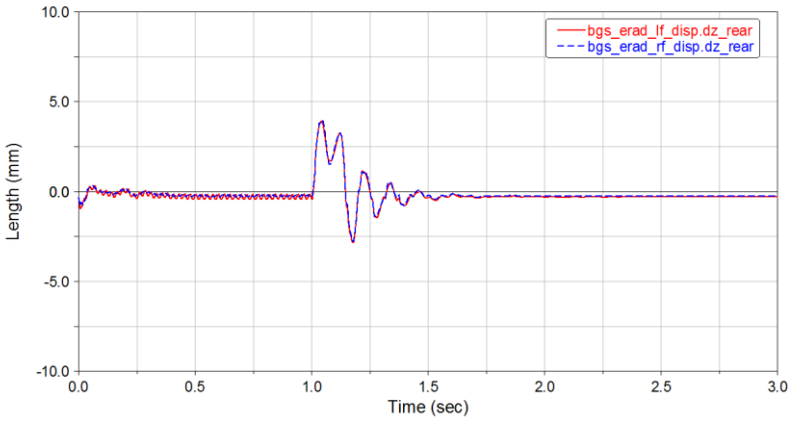


**Figure 3.8-3** Existing installation front bushing displacement

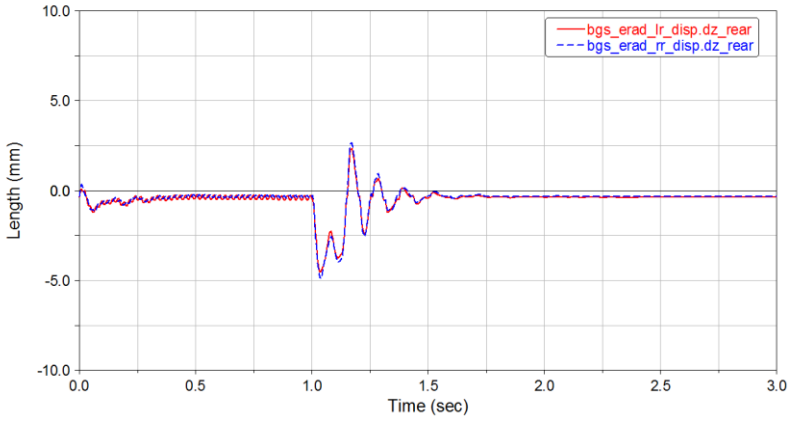


**Figure 3.8-4** Existing installation rear bushing displacement

Concept 5 was modeled by modifying the existing model (see figure 3.8-5). Mounting positions were changed according to table 3.7-1 and the fourth mount was removed (since the concept only consists of three mounts). Bushing stiffness was updated according to table 3.6-3).

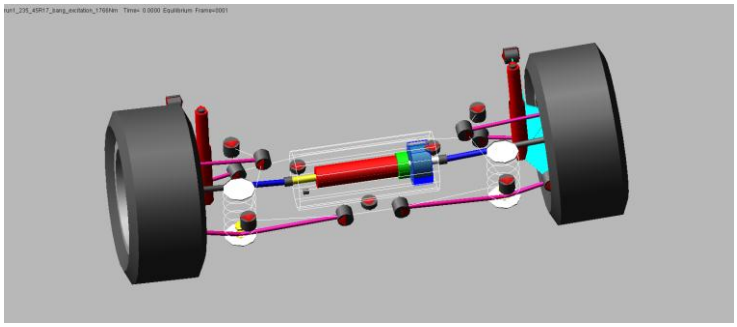

**Figure 3.8-5** Concept rear axle model in ADAMS

The model was then simulated with the same "Bang Oscillation" load case. Drive shaft torque behavior is shown in figure 3.8-6. The largest bushing deflections occurred in the x-direction and are shown in figure 3.8-7 and 3.8-8. Remaining directions are found in appendix D.

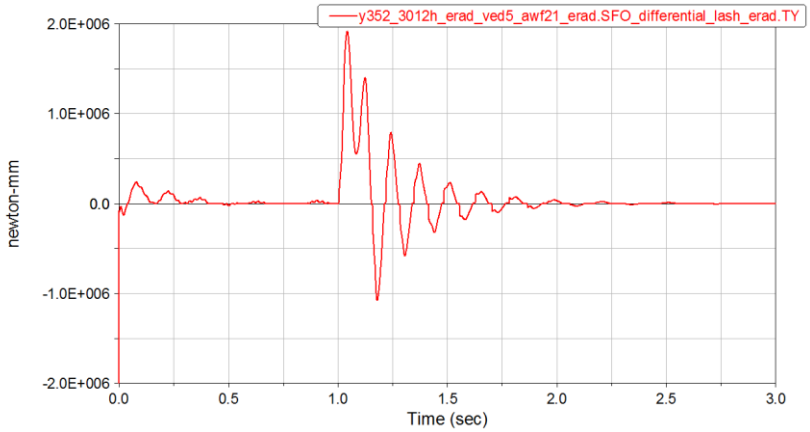


**Figure 3.8-6** Rear drive shaft torque excitation (concept installation)

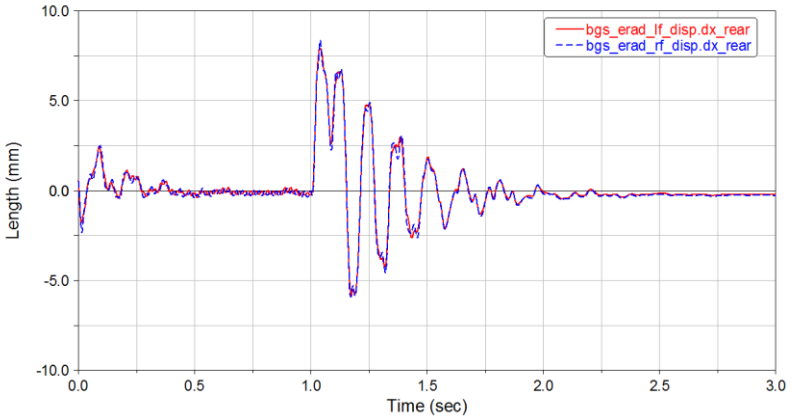


**Figure 3.8-7** Concept installation front bushing displacement

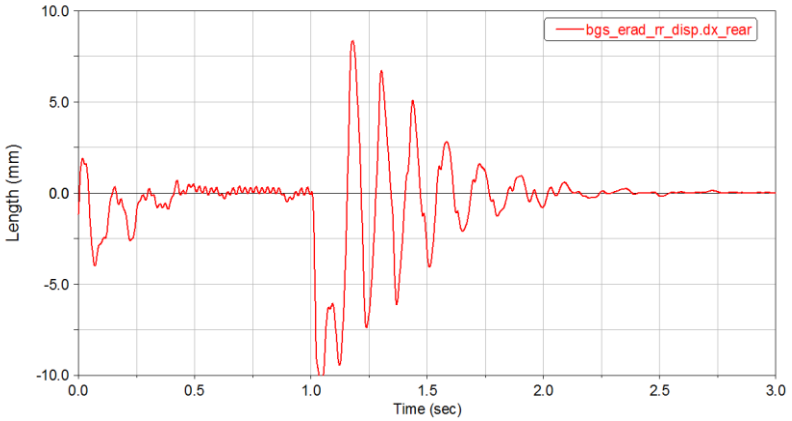


**Figure 3.8-8** Concept installation rear bushing displacement

The simulation shows large a large difference in bushing displacement for the existing installation compared to the concept layout. The maximum deflection for the existing installation is below 5 mm for both the front- and rear bushings. The concept installation shows displacements above 7.5 mm for the front mounts and reaches 10mm for the rear bushing. The existing installation transmits the torque mainly in the z-direction and the bushings are tuned for this behavior. The concept layout uses the same total bushing stiffness but the torque is instead mainly transmitted in the x-direction where the bushing stiffness is lower. Furthermore both concept bushings have shorter leverage arms causing higher mount forces and therefore more deflection.

### 3.9 Windup study

The ADAMS analysis for the concept design showed large displacements (>7.5mm) for both the side- and lower bushing. The displacements for the existing installations are below 5mm. This raised the question of how much windup that should be allowed for the ERAD. The existing installation is stiff in z due to drivability and interference constraints, causing high bushing stiffness and thus constraining the wind up. The concept design allows wind up tuning while z stiffness can be kept high to satisfy other constraints. A Matlab script was made to plot bushing displacement- and wind-up for the existing- and concept layouts. It is found in appendix E.

Free body diagram of the existing installation:

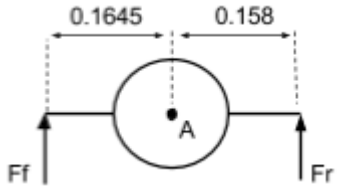


**Figure 3.9-1** Free body diagram of the existing installation (side view)

$$F_f * 0.1645 - F_r * 0.158 = 0 \quad (5)$$

$$F_f = \frac{0.158}{0.1645} F_r \quad (6)$$

The displacement for the front bushing (in mm) is given by:

$$u_f = \frac{F_f}{k_f} \qquad (7)$$

The displacement for the rear bushing (in mm) is given by:

$$u_r = \frac{F_r}{k_r} \qquad (8)$$

Finally, the wind-up is given by:

$$\alpha_{existing} = \sin^{-1}((u_f + u_r)/322.5) \qquad (9)$$

Free body diagram for the concept installation:

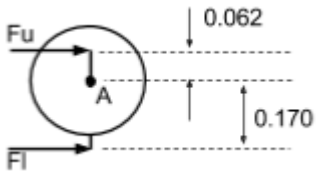


**Figure 3.9-2** Free body diagram of the concept installation (side view)

$$F_u * 0.062 - F_l * 0.170 = 0 \quad (10)$$

$$F_l = \frac{0.062}{0.170} F_u \quad (11)$$

The displacement for the upper bushing (in mm) is given by:

$$u_u = \frac{F_u}{k_u} \qquad (12)$$

The displacement for the rear bushing (in mm) is given by:

$$u_l = \frac{F_l}{k_l} \qquad (13)$$

Finally, the wind-up is given by:

$$\alpha_{concept} = \sin^{-1}((u_u + u_l)/232) \qquad (14)$$

At full brake pressure, approximately 2000 Nm is applied around A on the rear drive shafts (see figure 3.8-2 and 3.8-6). This results in a maximum windup of 1.3˚ for the existing installation. The largest bushing deflection occurs at the rear bushing and is 3.75 mm. The windup vs. torque for the existing installation is shown in figure 3.9-3. The bushing deflection vs. torque for the existing installation is shown in figure 3.9-4.

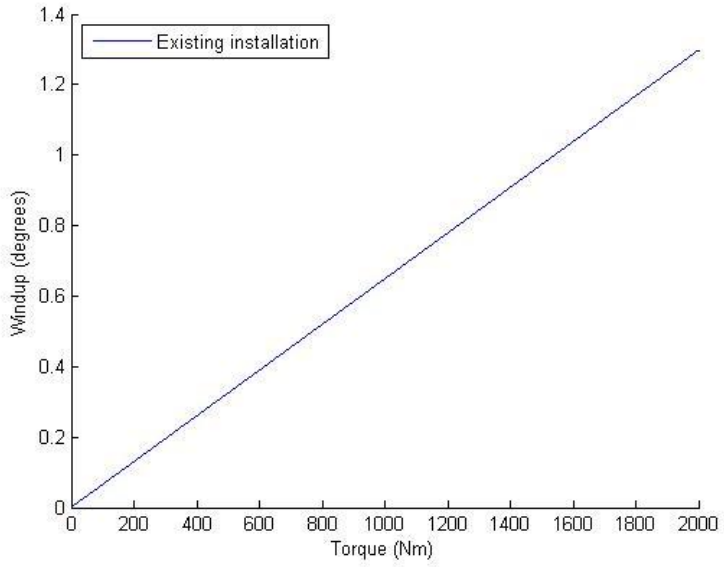


**Figure 3.9-3** Existing installation windup vs. torque

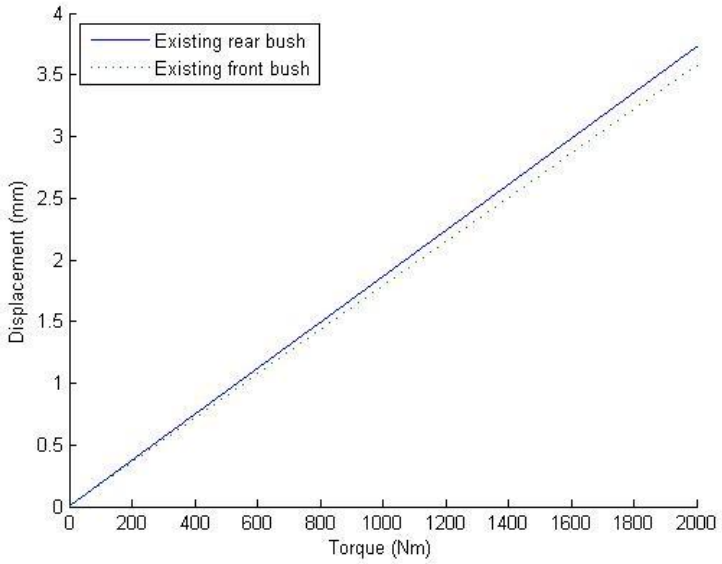


**Figure 3.9-4** Existing installation bushing displacement vs. torque

The wind-up vs. torque for the concept installation using the initial bushing setup is shown in figure 3.9-5. The bushing deflection vs. torque for the concept installation is shown in figure 3.9-6.

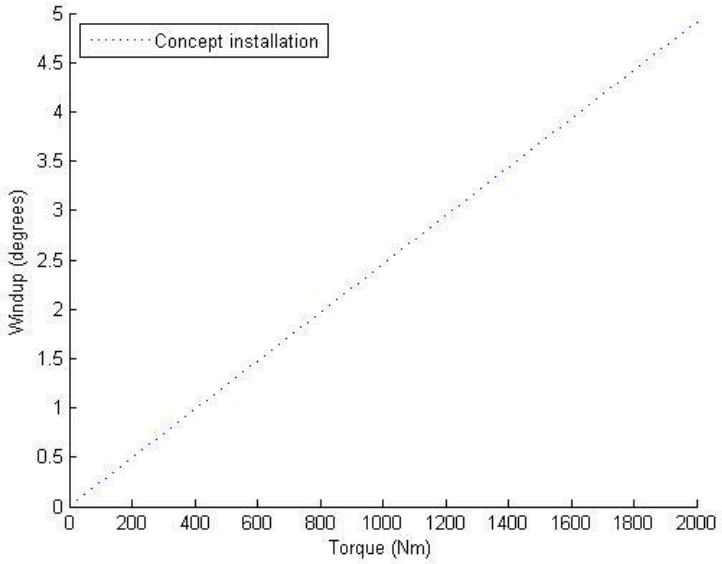


**Figure 3.9-5** Concept installation windup vs. torque

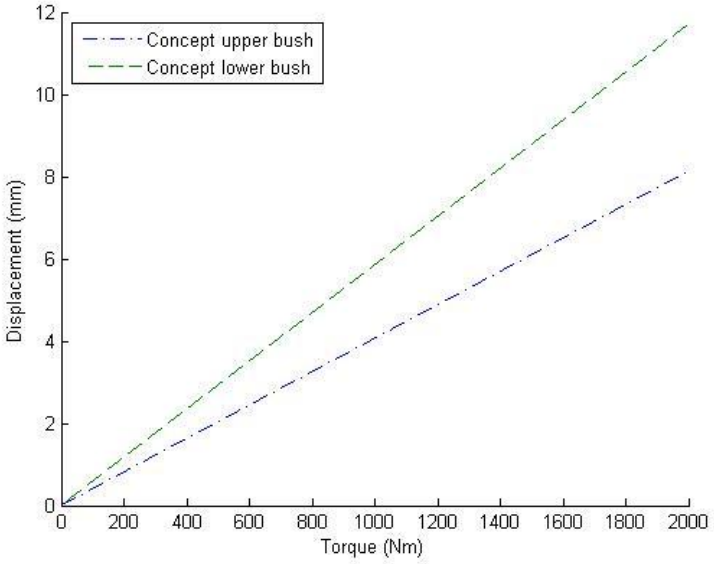


**Figure 3.9-6** Concept installation bushing displacement

The maximum windup for the concept installation is 4.9˚. This can be compared with Volvos regular diesel- and gasoline powertrains which are allowed to wind up 5˚. The largest bushing deflection occurs at the lower bushing and is 12 mm.

# 4 Results and discussion

*This chapter discusses the results of the project.*

## 4.1 Influence of design changes

The result of changing the z-coordinates for the side mounts due to drive shaft interference caused a different SPL at interior mic1. It is lower from 25 to 35 Hz and from 80 to 90 Hz. The rest of the frequency content is higher, around +5 dB from 35 to 65 Hz and almost +10 dB from 90 to 150 Hz.

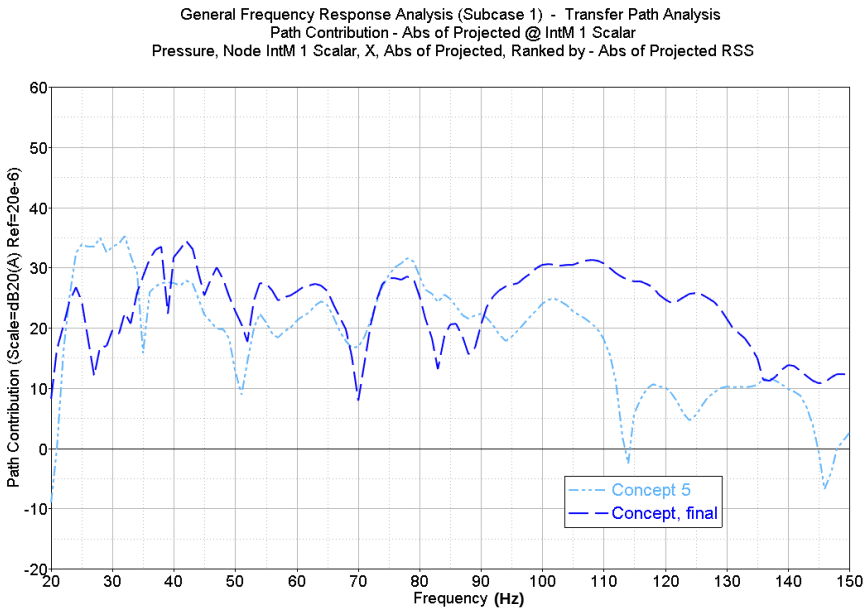


**Figure 4.1-1** SPL comparison between concept 5 and the updated concept from chapter 3.7

A comparison between the final concept and the existing installation is seen in figure 4.1-2. A lower SPL is obtained from 53 to 150 Hz while the frequencies below 53 Hz show a higher SPL. The maximum obtained SPL for the concept is 35 dB compared with 58 dB for the existing installation.

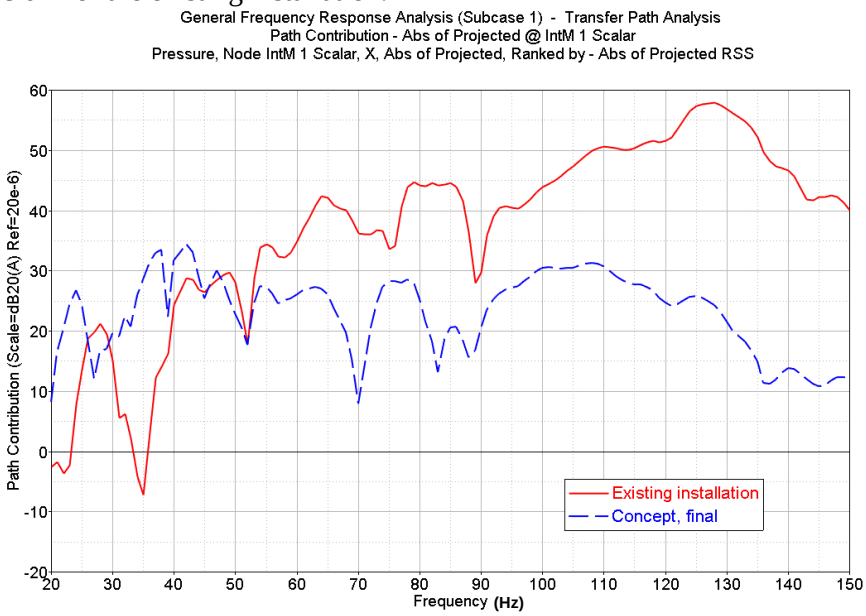


**Figure 4.1-2** SPL comparison between the final concept and the existing installation

## 4.2 Windup and bushing effects on SPL

It is difficult to compare two different installation layouts side by side, due to different windup and space constraints. The concept windup is 4.9˚ compared to the existing installation which windup 1.3˚. To see if the lower sound pressure level only is dependent on windup or if its layout dependent, the following study was made. The Matlab script was used to find bushing stiffness for the concept installation which result in a 1.3˚ windup. These were then applied in the CAE model and the SPL was obtained. Furthermore, the script was used to find bushing stiffness for the existing installation that results in a 4.9˚ windup. These were also used in the CAE model to obtain interior SPL.

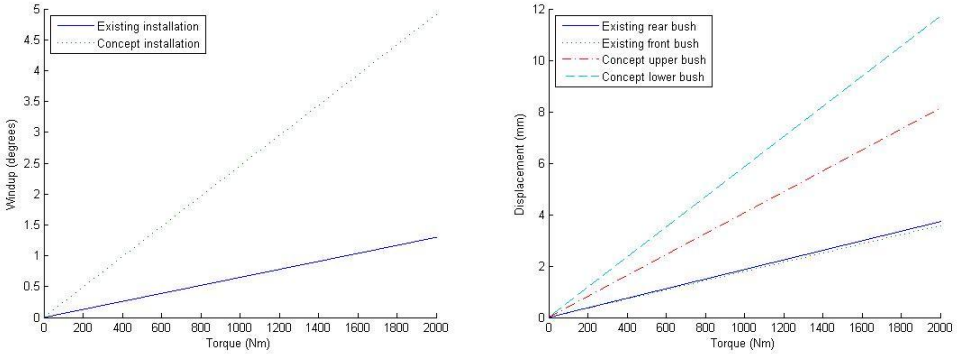


**Figure 4.2-1** Windup and bushing displacement comparison for concept- and existing layout

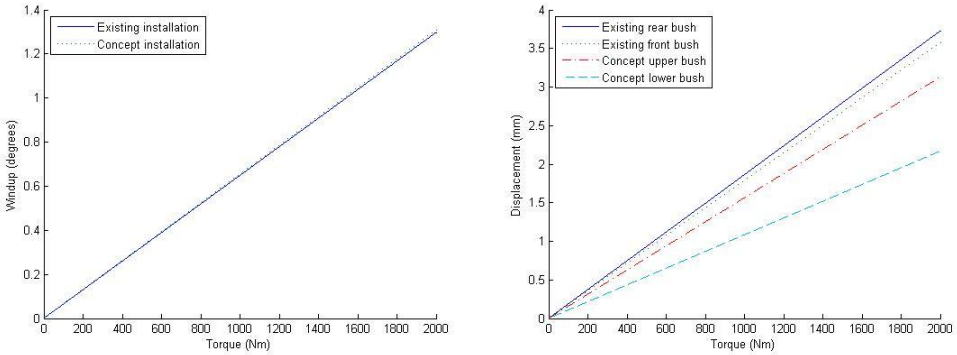


**Figure 4.2-2** Windup and bushing displacement comparison for concept- and existing layout with 1.3˚ windup

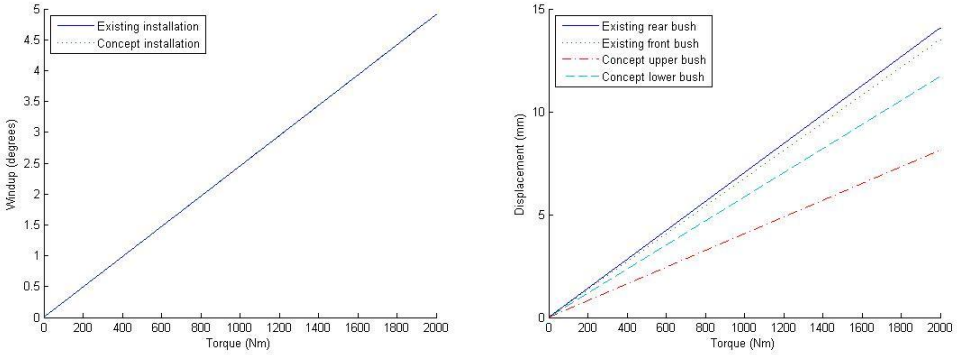


**Figure 4.2-3** Windup and bushing displacement comparison for concept- and existing layout with 4.9˚ windup

The bushing displacement is highly related to windup constraints, a larger windup results in a larger bushing displacement. Figure 4.2-1 shows a comparison between windup and bushing deflection for the initial windup, 1.3˚ for the existing and 4.9˚ for the concept. The result when both layouts are allowed to windup 1.3˚ is seen in figure

4.2-2. The concept upper bush deflects 3 mm and the lower bush deflects 2 mm. The 4.9˚ comparison is seen in figure 4.2-3 and shows displacements for the existing installation around 14 mm.

The sound pressure level with 1.3˚ windup comparison is shown in 4.2-4. The SPL has increased and is higher than the existing layout up to 63 Hz. Although a lower SPL is obtained above 63 Hz, but the difference has now decreased. The maximum obtained SPL is 45 dB for the concept compared with 58 dB for the existing installation.

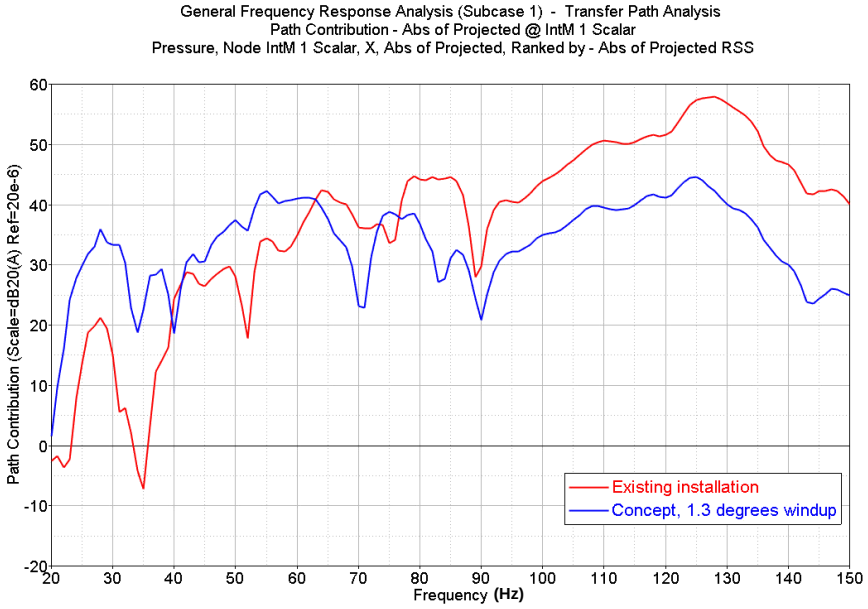


**Figure 4.2-4** SPL comparison between the final concept and the existing installation with 1.3˚ windup

With an allowed windup of 4.9˚, a lower SPL is obtained from 28 to 45 Hz for the existing installation. The SPL from 45 Hz and upwards is although lower for the concept installation by around 10 dB, which is shown in figure 4.2-5. The maximum SPL for the concept is 35 dB compared with 45 dB for the existing installation.

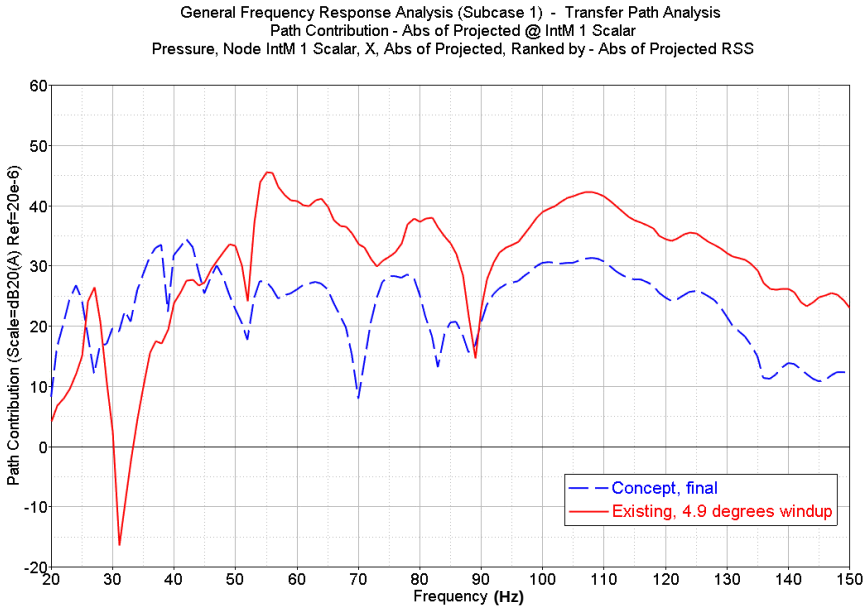


**Figure 4.2-5** SPL comparison between the final concept and the existing installation with 4.9˚ windup

## 4.3 Packaging limitations

Another important design factor is the packaging space and requirements. More space is needed to allow higher windup. Depending on the installation concept it maybe isn't possible to allow as much windup as wished to obtain good NVH. To give the reader an insight in how tight the packaging is for the concept layout, a section view of the lower torque rod is shown in figure 4.3-1. It allows around ±10mm deflection in the x-direction and around 5mm in z-direction before interference occurs. This has to be further evaluated if the concept layout is realized to prevent interference.

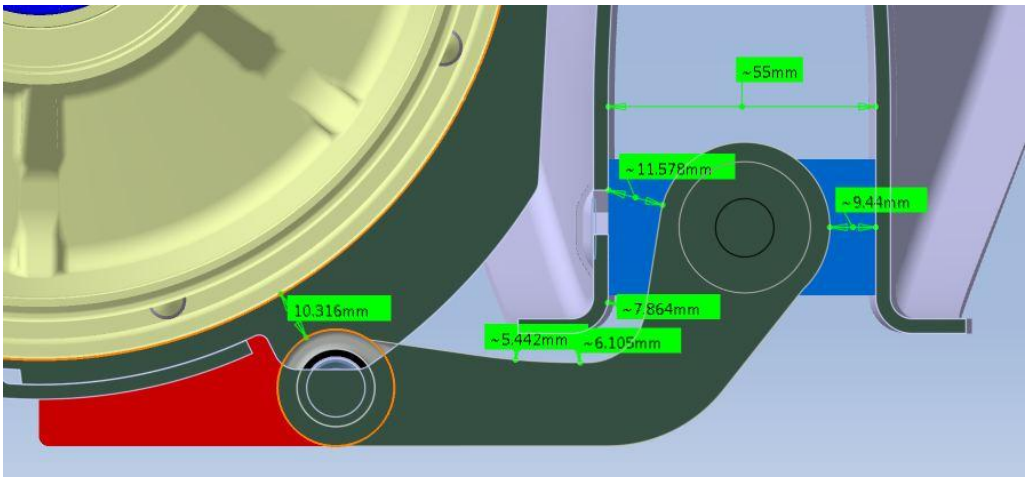


**Figure 4.3-1** Lower torque rod packaging space

## 4.4 Design comparison

The installation layouts are seen side-by-side in figure 4.4-1. They share the existing mounting points on the stator housing, but the concept layout is then mounted to the subframe at the sides instead through the surrounding structure. The rotation is restrained by the lower torque rod which is mounted onto the stator housing by welded brackets and located inside the rear subframe u-profile (seen in appendix C). Beside relocating the exhaust pipe and removing the existing four bushing mounts on the subframe, the coolant connections have to be modified. It is tight between the coolant connections and the surrounding structure (see figure C.7) and these probably have to be angled 90˚ so they point rearwards instead. The ERAD cable harness seen on the existing installation is assumed be moveable slightly upwards if interference with the surrounding structure occurs.

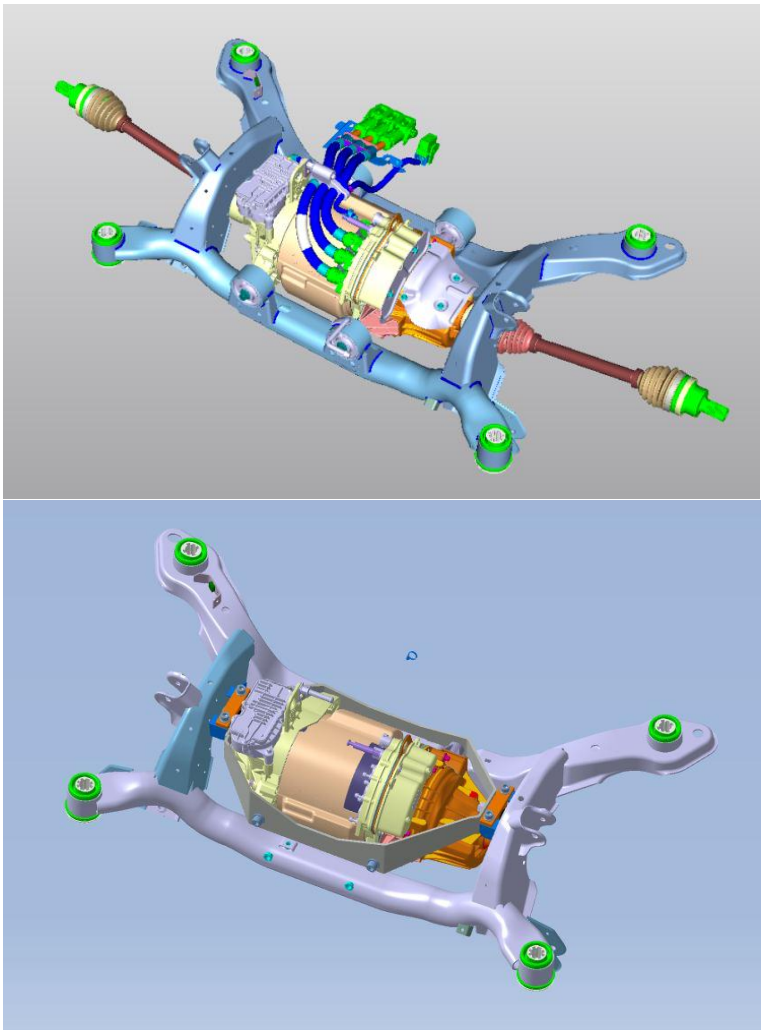

**Figure 4.4-1** Design comparison, existing (upper) and concept (lower)

# 5 Conclusions and recommendations

*This chapter contains the conclusions and recommendations for further work*

The main goal of this thesis was to try to find an installation for an electric motor which gives a lower SPL in the vehicle compartment. The results show that the concept layout gives a lower SPL than the existing installation between 63-150 Hz and a higher SPL below 63 Hz with the same allowed windup (1.3˚). The maximum SPL for the concept layout is 45 dB while the existing installation reaches 58 dB. The increase in SPL at the lower frequencies could increase low-frequency buzzing while the SPL decrease at higher frequencies could mitigate the tram-noise. Furthermore, the low frequency buzzing may be less heard due to masking effects from other vehicle systems e.g. road noise, but can also be perceived as more annoying. The results also show that the SPL is highly dependent on allowed windup, were more windup results in lower SPL for both the existing- and concept installation. An interesting result of the windup study is that the existing installation still shows higher SPLs with 4.9˚ windup. One advantage of the concept layout is that the windup can be tuned with less influence on interference constraints in z-direction compared to today's layout.

The concept calculations were made for only one vehicle model and an existing rear axle drive. Other vehicles may be less sensitive in the z-direction which has to be taken into account if the concept is to be implemented in other models. Furthermore the structure borne engine orders and motor behavior may change with a different ERAD. Since only the NVH aspects were discussed in this thesis, more studies with other aspects e.g. packaging and drivability have to be done in order to make sure that a change of installation layout is profitable as a long term solution.

The influence of the fifth order (which can be seen in figure 3.2-1) was discussed at the presentation. The conclusion, after discussion with David at Volvo, was that it isn't as prominent as the others and therefore probably not would affect the results too much. The prominent orders are mainly influenced by the design of the electric motor. The findings regarding this ERAD and its installation are that some orders of multiples of 5 are prominent.

My recommendation to Volvo is to further evaluate this with other aspects and manufacture a prototype that can be evaluated as a proof-of-concept. The prototype can be installed in an existing vehicle with minor modifications and at a relatively low cost.

# References

[1] Hatti, K., John Britto, V., and sankaranarayana, S., "NVH Attribute - Roadmap for Competitive Advantage," SAE Technical Paper 2013-01-2851, 2013.

[2] Afaneh, A., Abdelhamid, M., and Qatu, M., "Engineering Challenges with Vehicle Noise and Vibration in Product Development," SAE Technical Paper 2007-01-2434, 2007, doi:10.4271/2007-01-2434.

[3] Dupont, J., Bouvet, P., and Wojtowicki, J., "Simulation of the Airborne and Structure-Borne Noise of Electric Powertrain: Validation of the Simulation Methodology," SAE Technical Paper 2013-01-2005, 2013, doi:10.4271/2013-01-2005.

[4] Eisele, G., Wolff, K., Wittler, M., Abtahi, R. et al., "Acoustics of Hybrid Vehicles," SAE Technical Paper 2010-01-1402, 2010, doi:10.4271/2010-01-1402.

[5] B. Alzahabi, A. Mazzei, L.K. Natarajan, Investigation of Powertrain Rigid Body Modes, Kettering University

http://sem-proceedings.com/21i/sem.org-IMAC-XXI-Conf-s41p03-Investigation-Powertrain-Rigid-Body-Modes.pdf

[6] Sachdeva, D. and Hadi, R., "Effect of Engine Mounting Strategy on Vehicle NVH," SAE Technical Paper 2003-01-1467, 2003, doi:10.4271/2003-01-1467.

[7] Erdelyi, H., Roesems, D., Toso, A., and Donders, S., "Powertrain Mounting System Layout for Decoupling Rigid-Body Modes in the Vehicle Concept Design Stage," SAE Technical Paper 2013-01-1706, 2013, doi:10.4271/2013-01-1706.

[8] What is Transfer Path Analysis? (electronic)

http://www.plm.automation.siemens.com/en_us/products/lms/testing/transfer-path-analysis.shtml#lightview%26uri=tcm:1023-220904%26title=What-is-Transfer-Path-Analysis-Technical-Info-40282%26docType=.pdf

[9] A.T. Moorhouse, A.S. Elliott, T.A. Evans, In situ measurement of the blocked force of structure-borne sound sources, Journal of Sound and Vibration, Volume 325, Issues 4–5, 11 September 2009, Pages 679-685, ISSN 0022-460X, http://dx.doi.org/10.1016/j.jsv.2009.04.035.

(http://www.sciencedirect.com/science/article/pii/S0022460X09003794)

[10] Volvo V60 Technical Data (electronic)

http://www.volvocars.com/se/all-cars/volvo-v60/specifications/pages/technical-spec.aspx

# Appendix A: Measurement equipment

This appendix contains the specifications of the measurement equipment.

Frontend: LMS Scadas Mobile

Microphones: B&K 4189 ½”

Accelerometers: Dytran, PCB and B&K with 10 $\frac{mV}{m/s^2}$ nominal sensitivity

# Appendix B: Measurement data

This appendix contains measured NTFs and reconstructed responses for engine order 30 and 90.

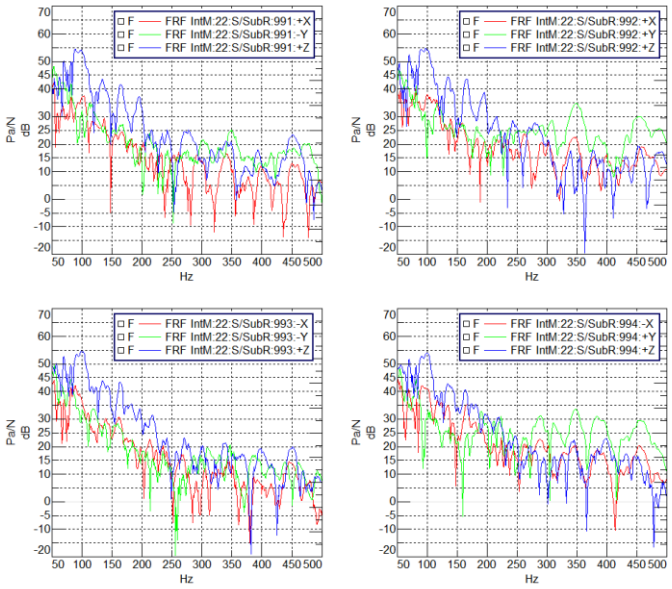


**Figure B.1** NTFs order 30

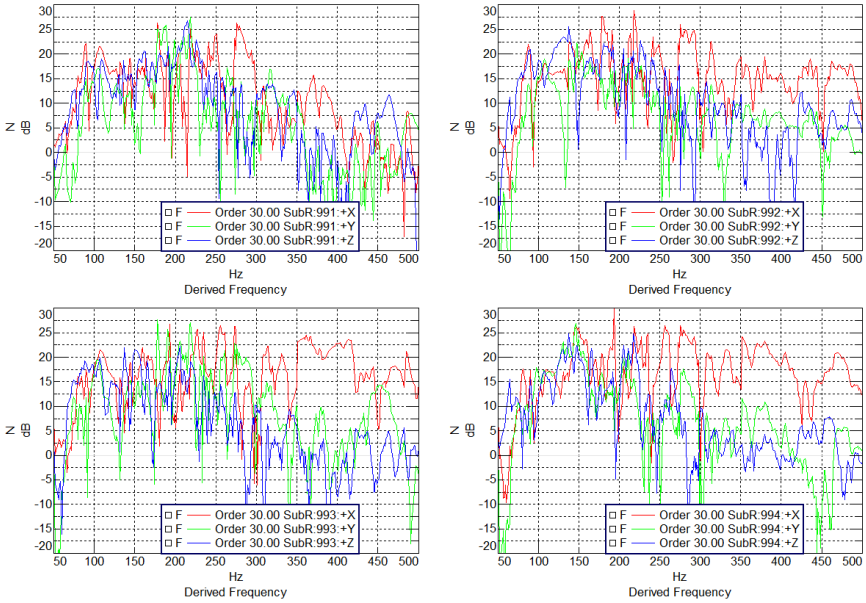


**Figure B.2** Engine order 30 calculated forces at the mounting points

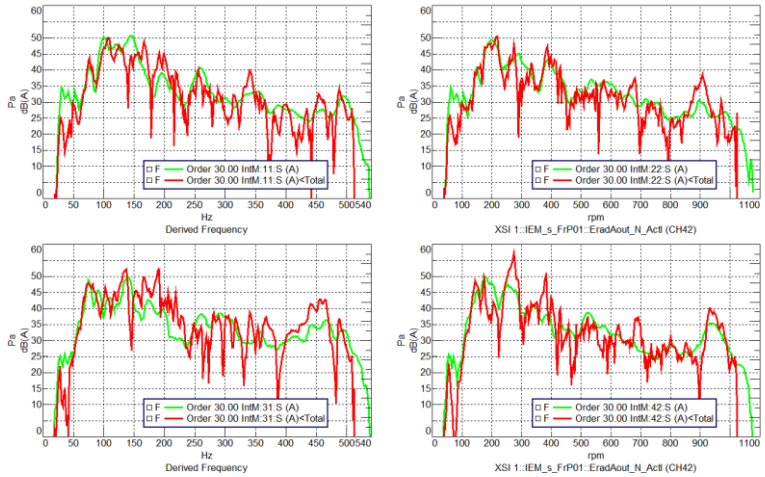


**Figure B.3** Order 30 measured vs. reconstructed response at microphones

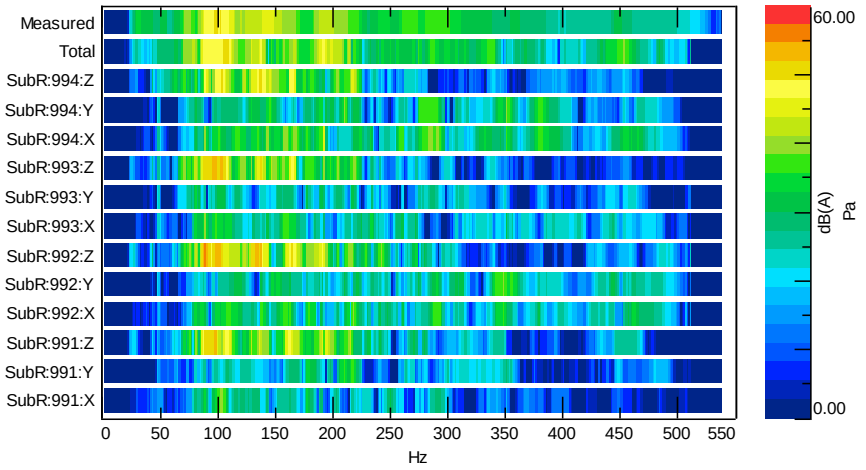


**Figure B.4** SPL contributors for engine order 30

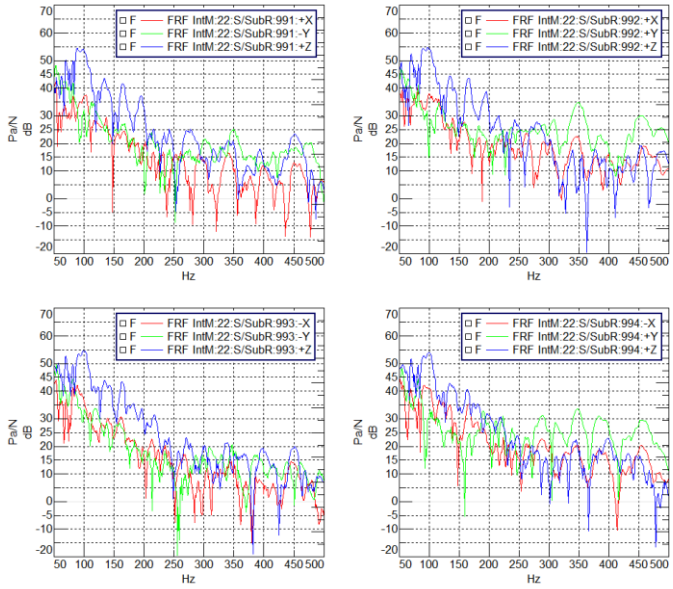


**Figure B.5** NTFs order 90

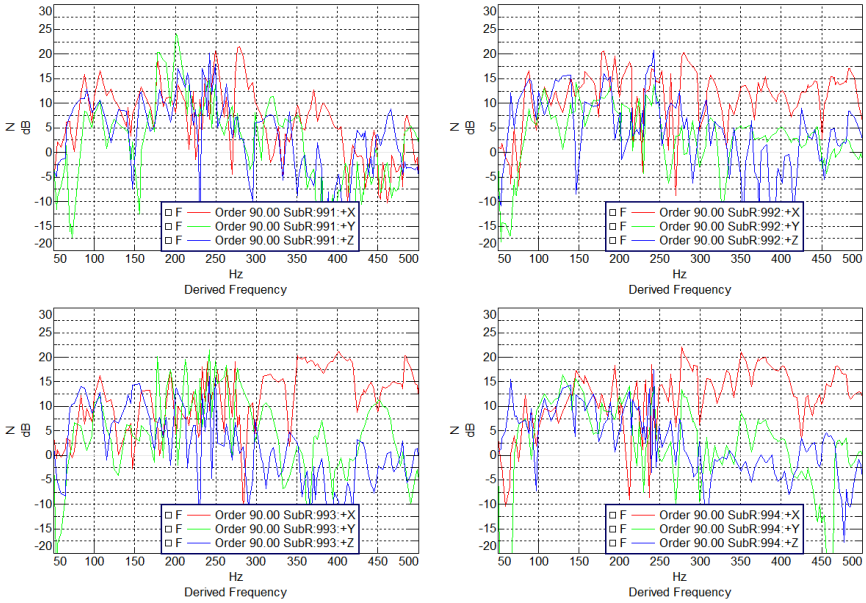


**Figure B.6** Engine order 90 calculated forces at the mounting points

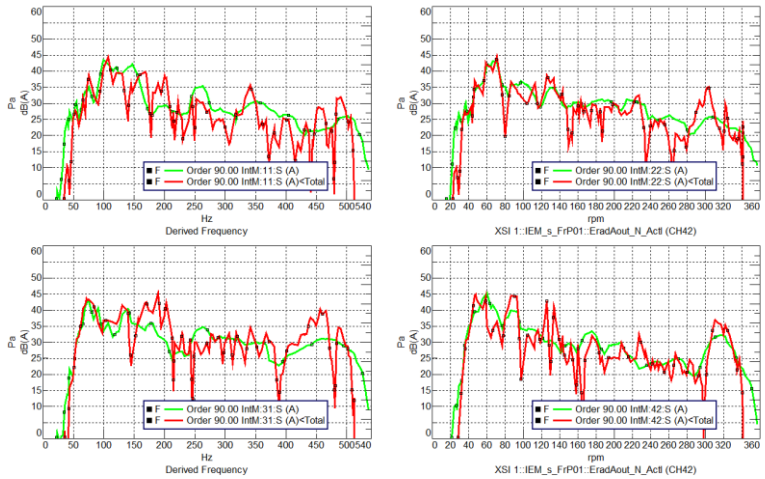


**Figure B.7** Order 90 measured vs. reconstructed response at microphones

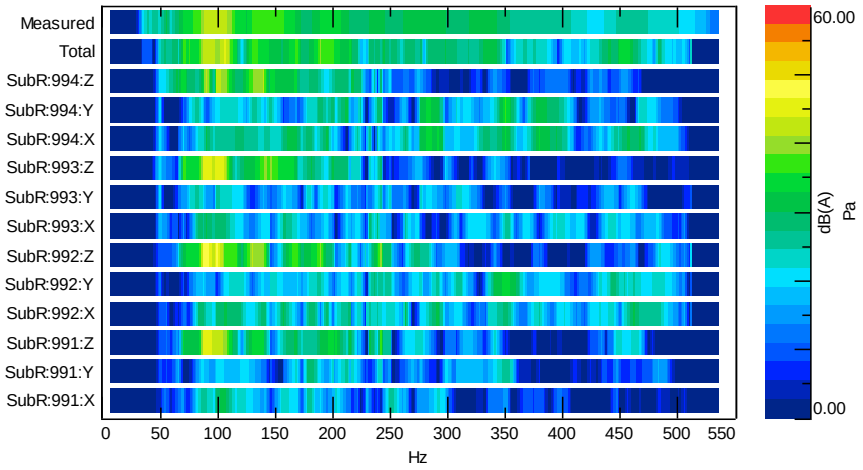


**Figure B.8** SPL contributors for engine order 90

# Appendix C: Concept installation

This appendix shows further views of the installation concept.

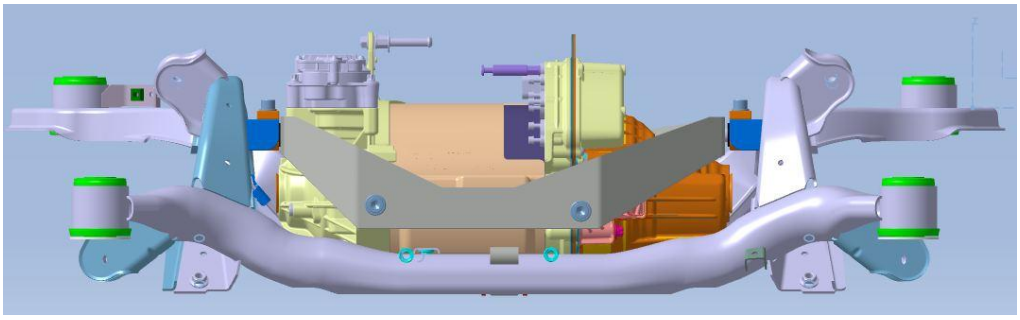

**Figure C.1** Concept installation front view

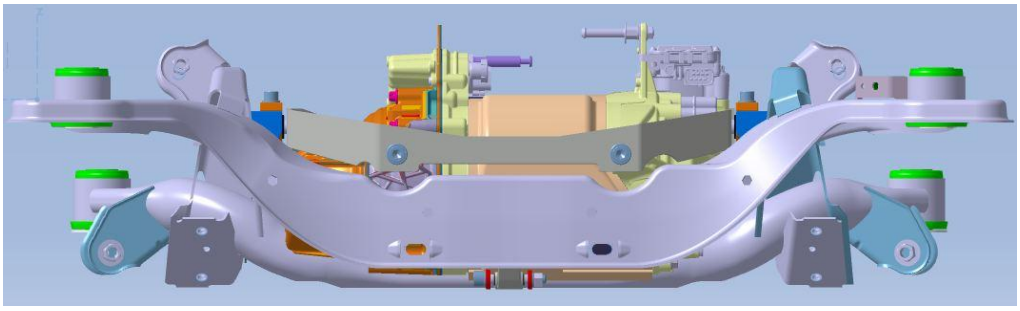

**Figure C.2** Concept installation rear view. Note the surrounding structure's geometry to prevent interference during windup

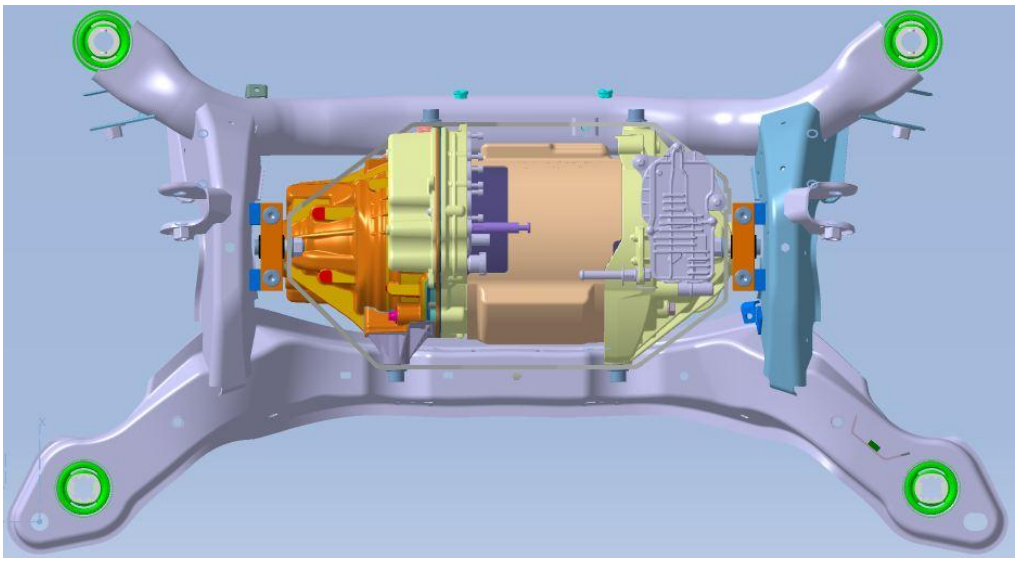

**Figure C.3** Concept installation upper view

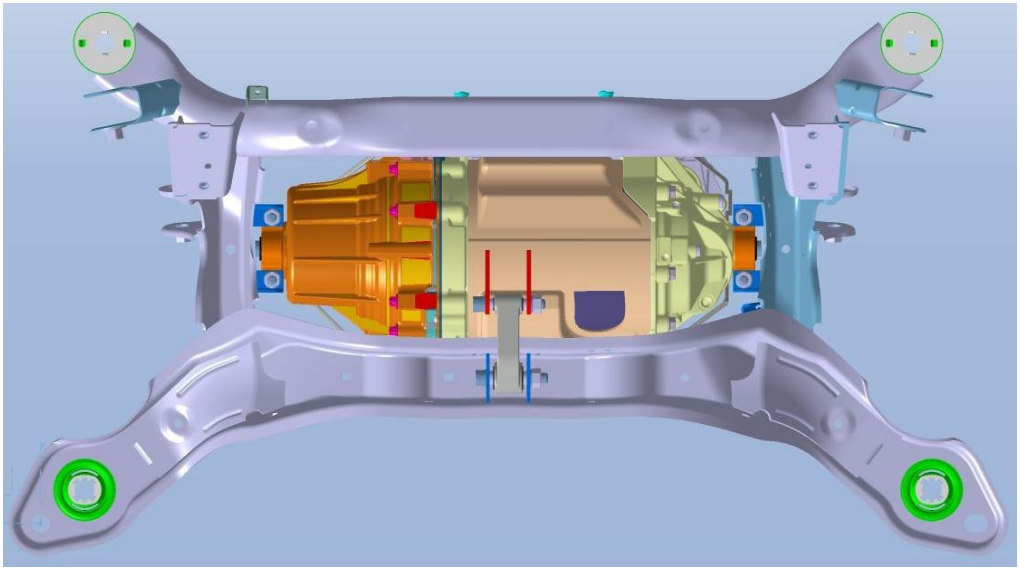

**Figure C.4** Concept installation bottom view

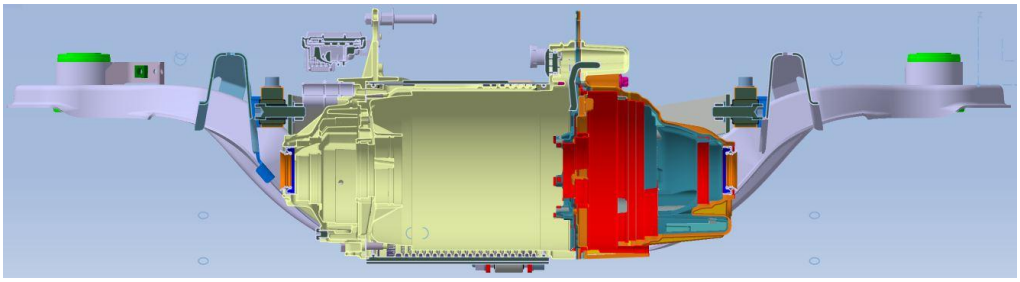

**Figure C.5** Concept installation front section view

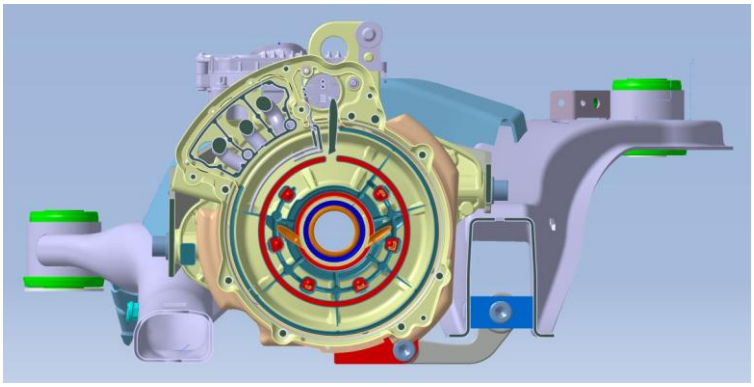

**Figure C.6** Concept installation left section view. Note the tight packaging of the torque rod due to ground clearance constraint

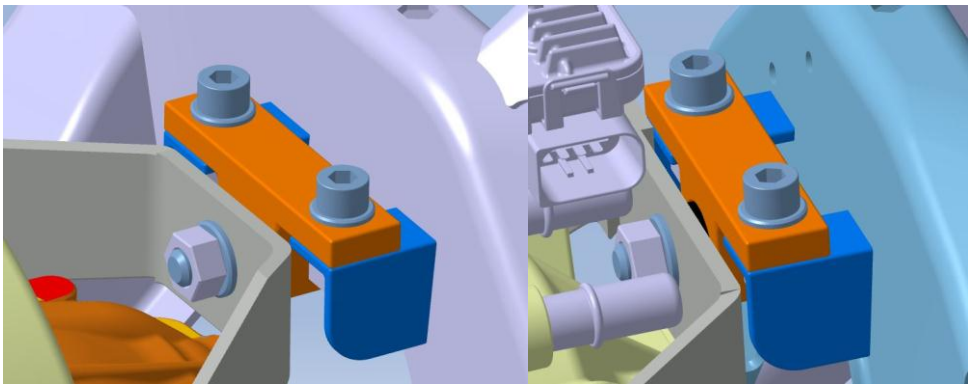

**Figure C.7** Concept installation left and right mount packaging. Note the coolant hose connections that need to be modified

# Appendix D: Bang oscillation simulation

This appendix contains bushing displacements for the remaining directions from the Bang Oscillation Simulation.

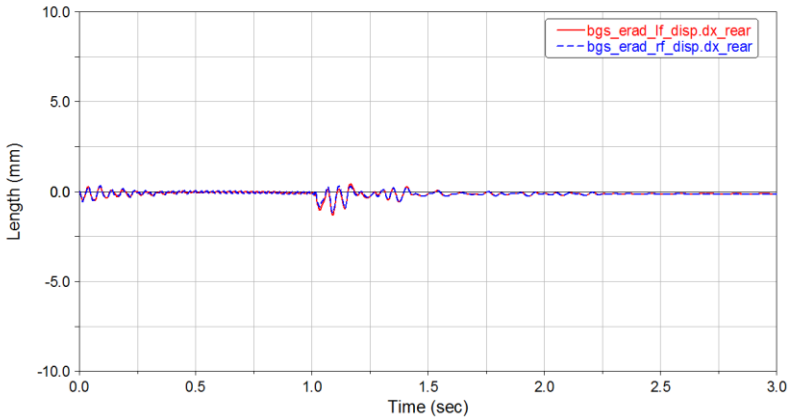


**Figure D.1** Front mount x-displacement for existing installation

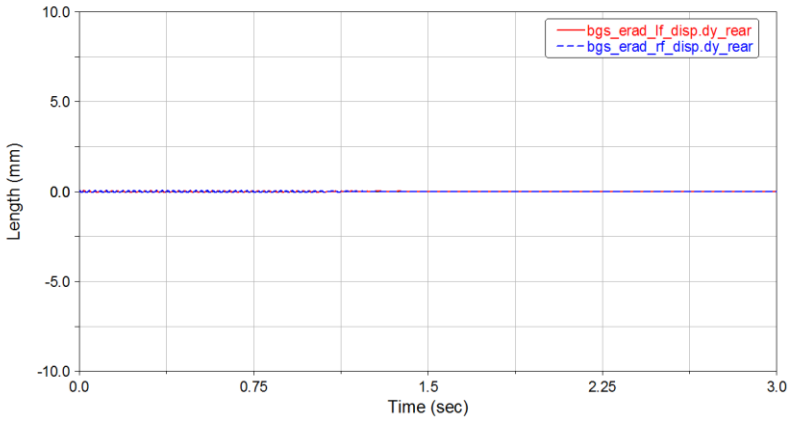


**Figure D.2** Front mount y-displacement for existing installation

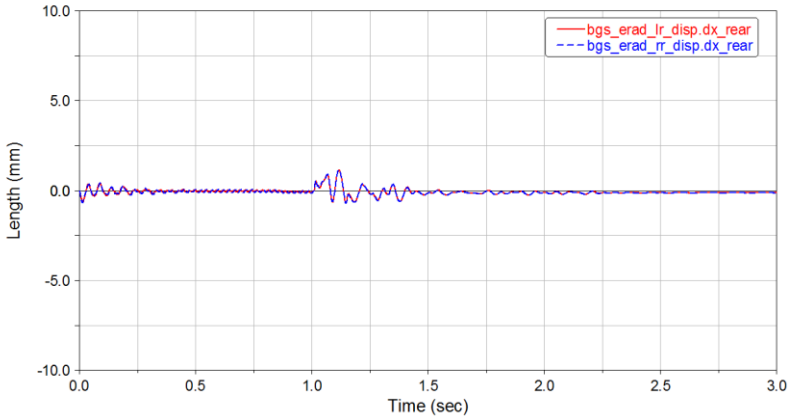


**Figure D.3** Rear mount x-displacement for existing installation

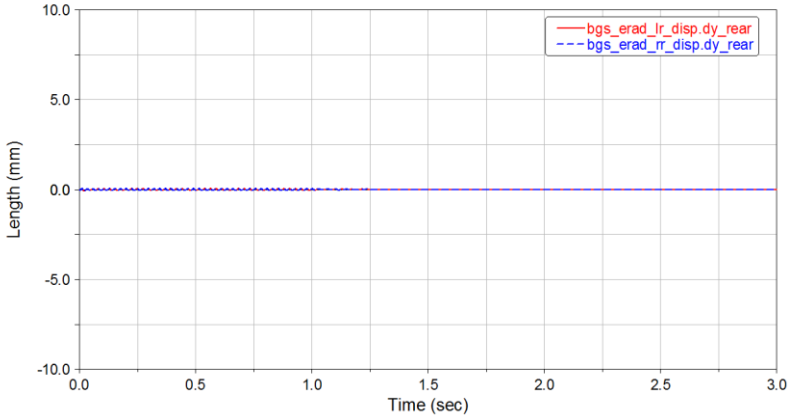


**Figure D.4** Rear mount y-displacement for existing installation

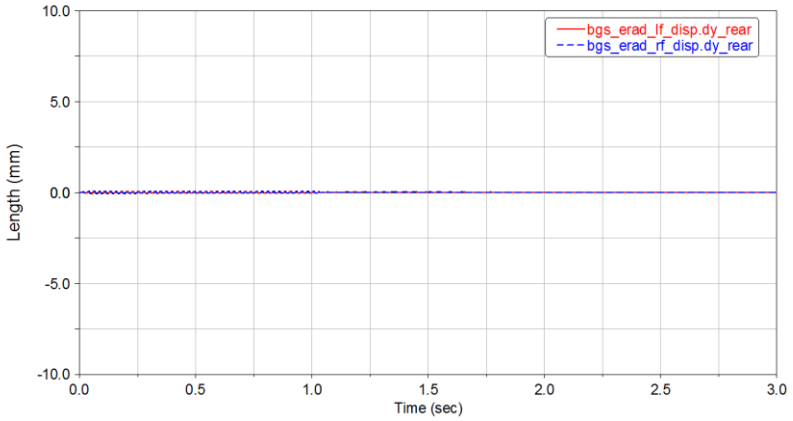


**Figure D.5** Front mount y-displacement for concept installation

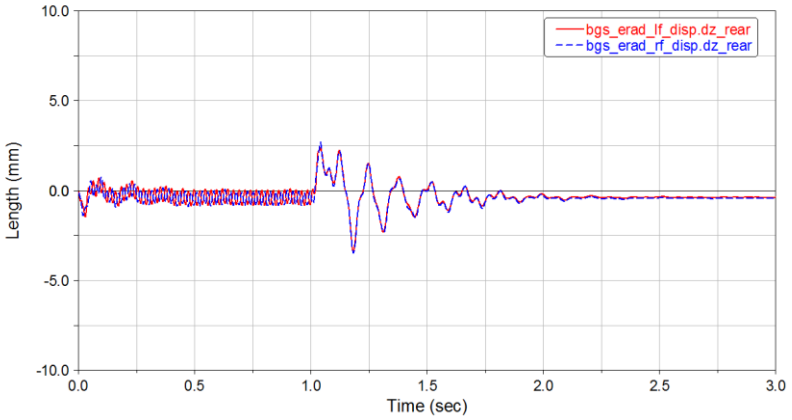


**Figure D.6** Front mount z-displacement for concept installation

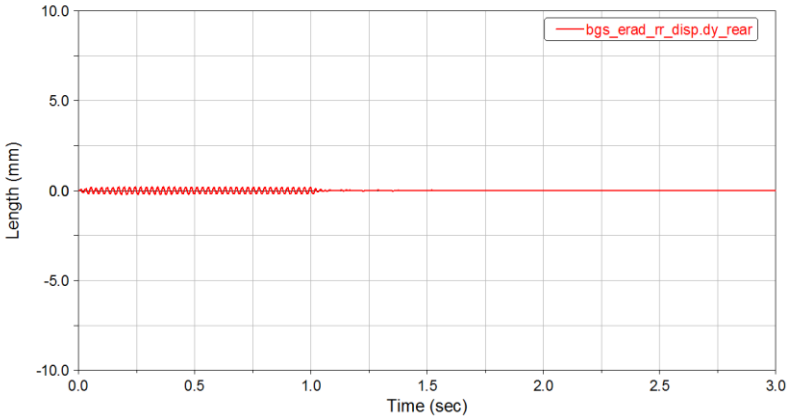


**Figure D.7** Rear mount y-displacement for concept installation

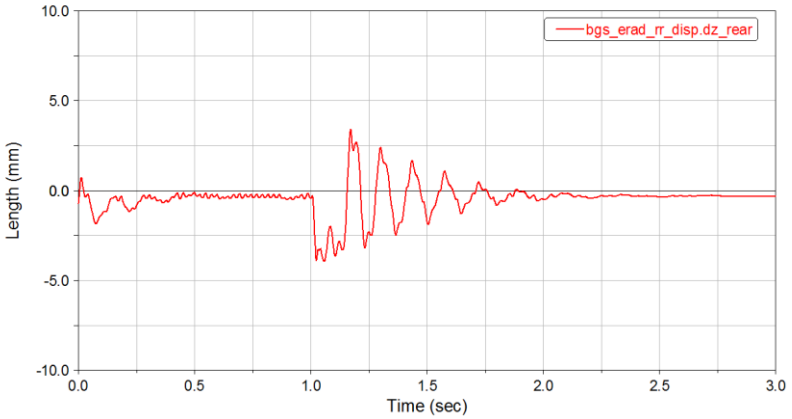


**Figure D.8** Rear mount z-displacement for concept installation

# Appendix E: Matlab script

This appendix contains the Matlab script to calculate windup.

```
close all
clear all

%%
torque=[1:1:2000];

%% existing
kz_r=850; %N/mm

kz_f=850; %N/mm

F_r=zeros();

F_r_bush=zeros();

F_f=zeros();

F_r_bush=zeros();

bush_disp_f=zeros();

bush_disp_r=zeros();

alfa_existing=zeros();

%% concept

kx_u=1000; %N/mm

kx_l=500; %N/mm

F_u=zeros();

F_n=zeros();

F_u_bush=zeros();
```

```
F_n_bush=zeros();

bush_disp_u=zeros();

bush_disp_n=zeros();

%% existing installation
for i=1:1:length(torque)

F_r(i)=torque(i)/(0.158+0.96*0.1645);

F_f(i)=F_r(i)*(0.96);

F_r_bush(i)=F_r(i)/2;

F_f_bush(i)=F_f(i)/2;

bush_disp_r(i)=F_r_bush(i)/kz_r;

bush_disp_f(i)=F_f_bush(i)/kz_f;

alfa_existing(i)=asind((bush_disp_r(i)+bush_disp_f(i))/322.5);

end
max(alfa_existing)

%% concept
for i=1:1:length(torque)

F_u(i)=torque(i)/(0.0618+0.17*0.36);

F_n(i)=F_u(i)*0.36;

F_u_bush(i)=F_u(i)/2;

F_n_bush(i)=F_n(i);

bush_disp_u(i)=F_u_bush(i)/kx_u;

bush_disp_n(i)=F_n_bush(i)/kx_l;

alfa_concept(i)=asind((bush_disp_u(i)+bush_disp_n(i))/231.8);

end
max(alfa_concept)
```

```
%% plot windup
hold all
plot(alfa_existing);
plot(alfa_concept,':');
legend('Existing installation','Concept
installation','location','northwest');
xlabel('Torque (Nm)');
ylabel('Windup (degrees)');

%% plot displacement
figure
hold all
plot(bush_disp_r);
plot(bush_disp_f,':');
plot(bush_disp_u,'-.');
plot(bush_disp_n,'--');
legend('Existing rear bush','Existing front bush','Concept
upper bush','Concept lower bush','location','northwest');
xlabel('Torque (Nm)');
ylabel('Displacement (mm)');
```

# Appendix F: Time plan review

The time plan for the thesis is seen in figure F.1. The project started week 4 and was supposed to presented and handed in by week 25. The time plan was made the first week to have something to aim for. The project followed the plan approximately with some minor differences. New questions arose during the execution which led to more theoretical studies. The preparation section which mostly included to get a basic understanding of the Hyperworks software and the FEM-model was less an own section and instead more integrated with the execution. The NVH Director software was something new for both me and my supervisor which led to many (and sometimes time consuming) questions. Furthermore the report writing was done in intervals e.g. one section was written when the theoretical study was made and another when the concepts were generated. Although the project was finished in time, the most time consuming part was the report writing the last weeks, which probably could have started earlier.

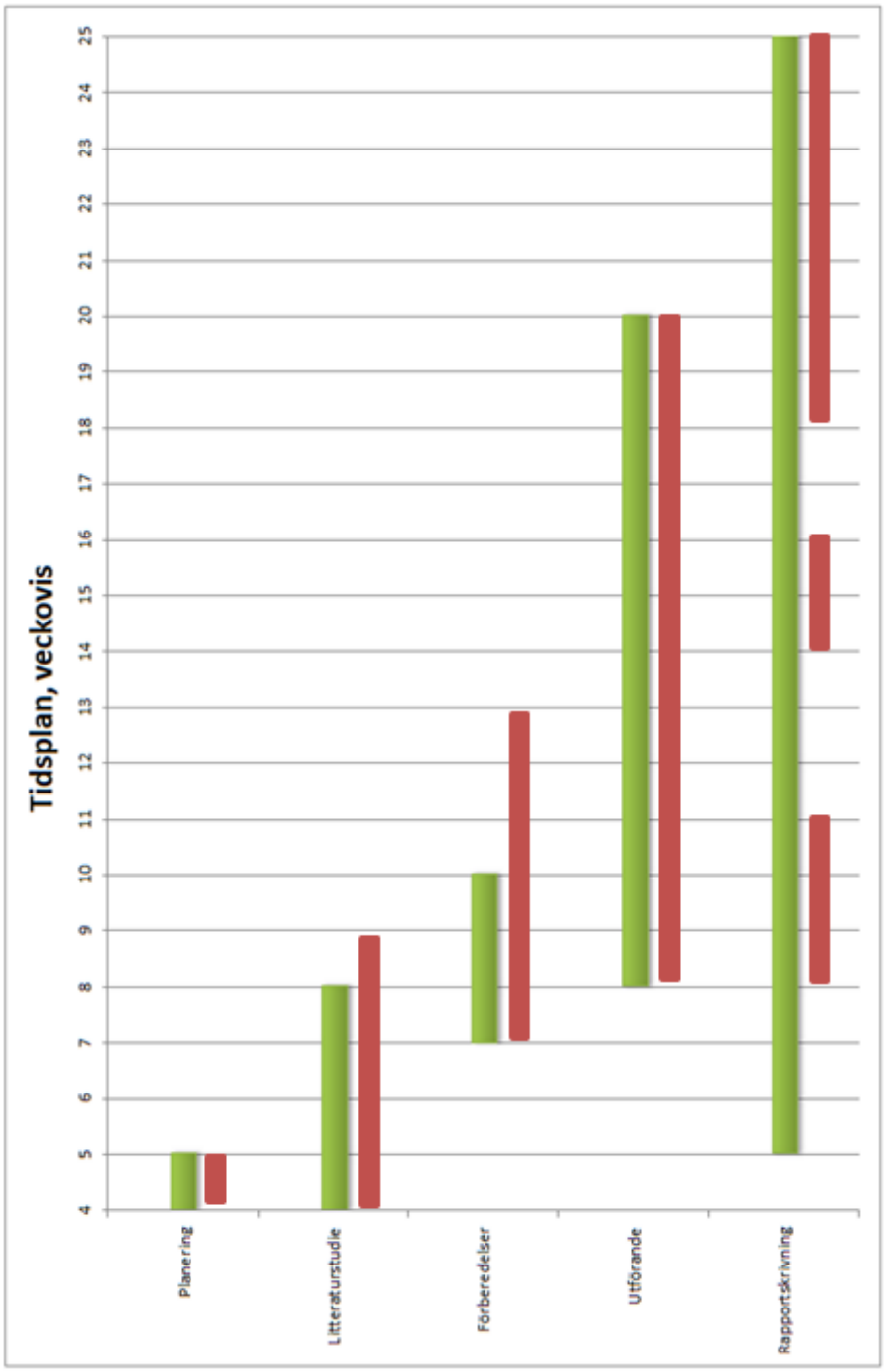


**Figure F.1** Time plan, initial schedule in green, actual schedule in red